RESEARCH ARTICLE

Ground motion hazard of the China–Pakistan Economic Corridor (CPEC) routes in Pakistan

Qasim Ur Rehman[1,2*], Muhammad Waseem[3], Waqas Ahmed[1], Ihtisham Islam[1,4], Hammad Tariq Janjuhah[4*] and George Kontakiotis[5]

Abstract

Pakistan has seen a burst of infrastructure development recently due to the increased connection between Asia and East Europe. The China–Pakistan Economic Corridor is a project between China and Pakistan aimed to improve the regional infrastructure that would ultimately enhance the connection between Asia and Eastern Europe. However, the active tectonics of Pakistan could put this infrastructure at risk if it is not built to the highest hazard prevention standard. This study reports the ground motion hazard by using the probabilistic seismic hazard assessment approach and the areal seismic source model. The seismic hazard maps of the China–Pakistan Economic Corridor in Pakistan are derived using the Cornell–McGuire (1968–1976) approach, which takes into account all earthquakes (25AD-2020) that occurred in Pakistan and nearby regions, the newest ground motion prediction equations, and an updated seismo-tectonic source model of Pakistan. The final ground motion intensities are attained as peak ground acceleration and 5% damped spectral acceleration at $T = 0.2$ s and 1.0 s for 475- and 2475-year return periods (estimated for bedrock site conditions). The results are displayed as color-coded maps that represent the amplitude deviation of ground motion. From the spatial evaluation of the maps, a peak ground acceleration value of 0.40–0.52 g for the 475-year return period and a spectral acceleration (0.2 s) value of 1.66–2.13 g for 2475-year return period are mostly observed on the northern and western routes. The central and eastern routes are mostly characterized by a peak ground acceleration value of 0.22–0.24 g for the 475-year return period and a spectral acceleration (0.2 s) value of 0.95–1.13 g due to diffused seismicity and lower number of faults in this region. The ground motion intensity values obtained in this study can be utilized for the seismic design of all kinds of infrastructure and bridges along the CPEC routes in accordance with the Building Code of Pakistan, the International Building codes, and the load and resistance factor design codes published by American Association of the State Highway and Transportation Officials.

Keywords Probabilistic seismic hazard, Seismic design, Areal source model, PGA and SA, CPEC route

*Correspondence:
Qasim Ur Rehman
qrehman@uoh.edu.pk
Hammad Tariq Janjuhah
hammadtariq013@gmail.com
Full list of author information is available at the end of the article

1 Introduction

Pakistan has a unique geographical location on the world map. It has transportation links with its neighbors (China, India, Afghanistan, and Iran), and the Arabian Ocean connects it to the rest of the world in the south. The China–Pakistan Economic Corridor (CPEC) project is the infrastructure program that will link Central Asia and Europe through Pakistan. The project includes such as upgrading highways, constructing 125 miles of tunnels, establishing a 2000-mile railway track from Kashgar to Gwadar, upgrading Gwadar airport, oil and gas pipelines, power grids, and related infrastructure that link China with Asia, Europe, the Middle East, Africa, and beyond (Irshad 2015). The highways will act as a channel for connecting billions of people across Asia, Africa, and Europe. Its main goal is to improve transportation between China and other regions, boosting trade and economic growth (Makhdoom et al. 2018; Tong 2014). However, the global disaster database specifies that the African, European, and Asian countries have twice the comparative average disaster damages. Primarily, the impact is ten times higher in southern and eastern Asia than the worldwide average (Chang et al. 2021). The highways in Pakistan are vulnerable owing to the active tectonics of the region, topographic relief, geologic structure, human engineering activity, and ground motion hazard (Fig. 1). The most frequent geologic hazards in the region are slope failures, erosion, avalanches, earthquakes, and landslides (Rehman et al. 2021). The landslides adversely affect the people and economy by abolishing the transportation system, buildings, and major infrastructure projects. On January 4, 2010, north Pakistan experienced a devastating Attabad landslide that blocked the Hunza River and created a dam upstream. According to the National Disaster Management Authority report of July 2010, about 16 km of the Karakoram Highway, i.e., part of the existing CPEC route, was buried, over 115 houses were destroyed, and 20 people were missing (Karim et al. 2015). Consequently, the region faced a slowdown in trade between Pakistan and China, which was about US\$ 8.7 billion before the disaster (Cook and Butz 2015). The Pakistan has also experienced a significant number of earthquakes with varying focal depths and moment magnitudes (M_w) > 7.0. On October 8, 2005, a massive earthquake of M_w 7.6 hit Pakistan and destroyed the transportation networks, communication services, infrastructure, farm fields, and electricity systems. Over 73,000 people died and 3.5 million were left homeless as a result of this earthquake (Fujiwara et al. 2006). The earthquake resulted in the triggering of various landslides in the vicinity of the epicenter location near Muzaffarabad and Balakot. The Hattian Bala landslide having volume 68×10^6 m³ was triggered by the

Kashmir 2005 earthquake and killed more than 1000 people (Basharat et al. 2012). Additional major earthquakes in the region include the 1819 Allah band, 1931 Mach, 1935 Quetta, 1945 Makran, 1997 Harnai, 2001 Bhuj, 2005 Kashmir, 2008 Awaran, 2011 Dalbandin, and 2013 Saravan (Bilham 1999; Bilham et al. 2007; Waseem et al. 2019). This series of earthquakes has resulted in numerous fatalities and infrastructural damage, revealing poorly constructed structures and inadequate seismic designs (Naseer et al. 2010). These hazards slow down the economies of developing countries such as Pakistan through loss of human lives and by destruction of infrastructure (Rehman et al. 2014). The earthquakes with M_w > 6.5 represent the recurrence of future major earthquakes in the region (Monalisa and Jan 2007). Therefore, it is necessary to assess the ground motion hazard of the transportation routes connecting China and Pakistan.

An accurate seismic hazard assessment is a step toward reducing the impact of future earthquakes. Damages can be mitigated by advising on earthquake-resistant design, seismic vulnerability, and regional loss evaluation models. A probabilistic seismic hazard analysis (PSHA) is a useful quantitative tool for estimating the uncertainty in the size, location, and ground motion intensity of future earthquakes in a region and identifying communities at risk from a seismic hazard. The goal of PSHA is to quantitatively estimate, on a probabilistic basis, how much shaking (seismic hazard) a site is likely to experience from future earthquakes. The method predicts the ground motion intensity at a given location. The probability density function (PDF) is used to model the deviation in ground motion. The rate of earthquakes is then computed by taking into account the ground motion measurements in relation to the threshold magnitude. The PSHA produces a curve of ground motion amplitudes according to the annual rate. Pakistan's seismic hazard assessment has been the subject of collaborative efforts by various organizations and researchers who have utilized a wide range of approaches. These include the research conducted by Ministry of housing and works for building code of Pakistan (BCP 2007) and by other researchers (Mahmood et al. 2020; Monalisa and Jan 2007; Rafi et al. 2012; Sesetyan et al. 2018a; Waseem et al. 2020; Waseem et al. 2019; Waseem et al. 2018; Zaman et al. 2012; Zhang et al. 1999). The factors that contribute to the variety of adopted approaches in these studies include: (1) the selection of ground motion prediction equations (GMPEs) for the region due to the lack of specialized GMPEs for this tectonic regime; (2) the consideration of shallow focus (focal depth up to 50 km) or deep focus (focal depth greater than 50 km) earthquakes or both; (3) the choice of a seismotectonic model based on active fault zones and data (Rahman et al. 2019; Sesetyan
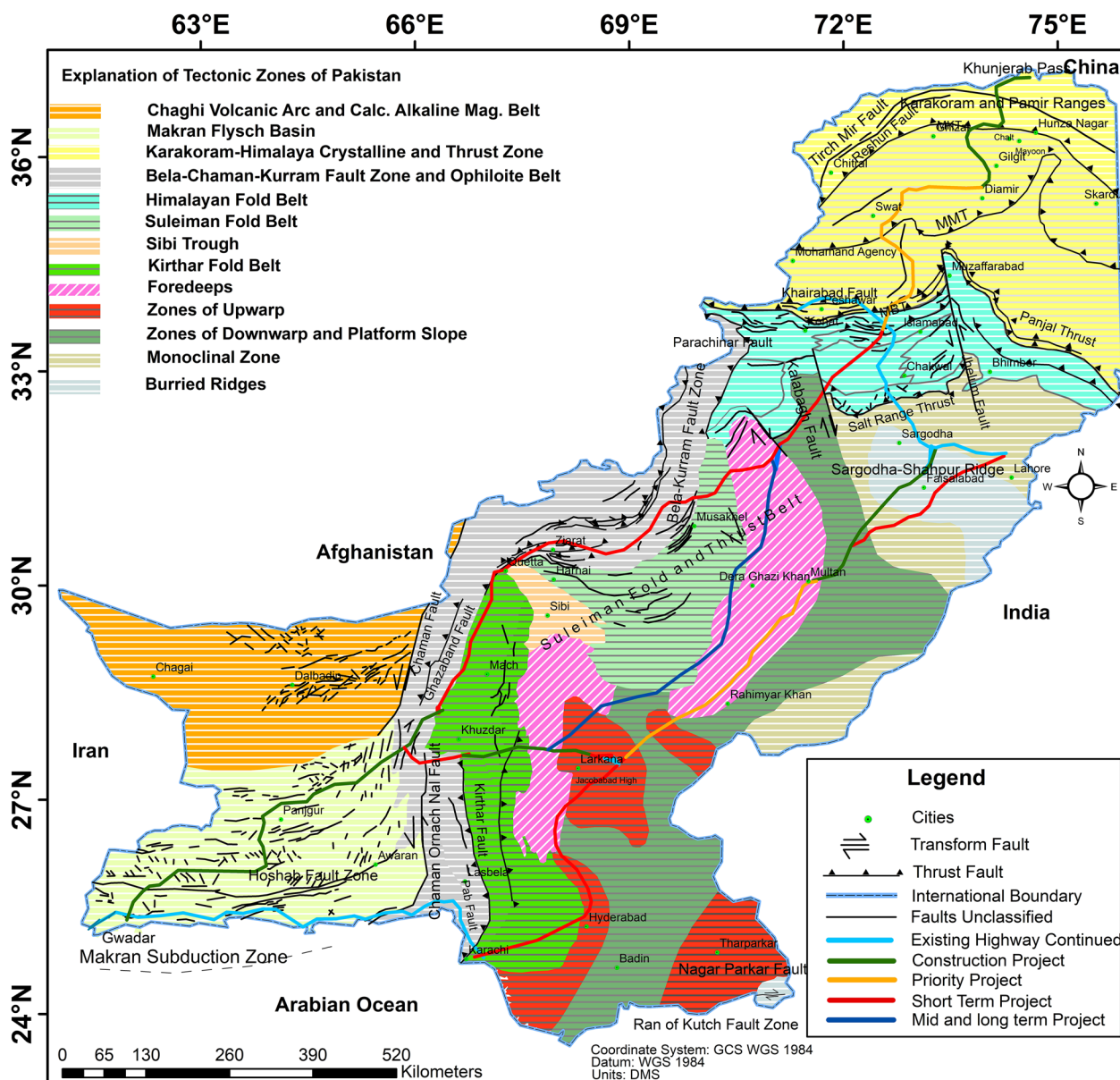
Rehman *et al. Progress in Earth and Planetary Science*   (2023) 10:27

Page 3 of 31

Fig. 1 The China–Pakistan Economic Corridor (CPEC) routes overlaid with the major tectonic zones of Pakistan, including the Chaman, Indus Suture, Main Mantle Thrust, and Karakoram Fault systems. The figure highlights the potential seismic hazards associated with the CPEC routes, as they traverse through seismically active regions with high rates of tectonic activity

et al. 2018b; Waseem et al. 2020); (4) the availability of a variety of methodologies, such as Cornell (1968), McGuire (1976), and the kernel estimate method (Rafi et al. 2012; Waseem et al. 2020, 2019, 2018; Zaman et al. 2012) for seismic hazard assessment. The specialized GMPEs are not derived from the tectonic regime of Pakistan. Therefore, the present study has utilized the four random GMPEs from the set of established equations developed for the similar tectonic regions of the world, considered both the shallow and deep focus earthquakes,

an updated areal seismotectonic model of Pakistan, and employed the Cornell–McGuire approach. This approach considers a constant seismicity rate that does not change in the identified seismic sources. Other advantages of choosing this standard approach for the present study include: (1) the availability of a limited-time earthquake catalog; (2) fault characterization in Pakistan is not very good; and (3) the ability to effectively assess the maximum magnitude potential of seismic sources.

The highway network between China and Pakistan is linked by several bridges over the Indus River and its major tributaries. The seismic design of all infrastructure, and particularly the bridges, requires spectral intensities in compliance with 2012 specifications of the American Association of State Highway and Transportation Officials (AASHTO 2012) and International Building Code (IBC) 2021 (Ching and Winkel 2021). The research evaluates the CPEC routes in Pakistan for all types of infrastructure in terms of peak ground acceleration (PGA) and spectral acceleration (SA) responses so that adequate structural engineering mitigation measures may be implemented in time to make this economic route productive. The paper specifically examines the seismic hazard risk qualitatively in terms of PGA and SA values at $T = 0.2$ s (short-period) and 1.0 s (long-period) for 475 years (10% probability of exceedance in 50 years) and 2475 years (2% probability of exceedance in 50 years)

RPs, respectively. This is accomplished by incorporating all the required input parameters into the OpenQuake version 3.10 software engine (Pagani et al. 2023) for hazard computation (Fig. 2).

2 Geologic and tectonic settings of Pakistan

Pakistan lies in a complicated tectonic setting with three active mountain ranges (Karakoram–Hindukush–Himalaya) intersecting in the north and an active tripe plate boundary (Indian–Arabian–Eurasian) in the south and southwest. In the middle section, lies the Sulaiman fold belt, formed by the oblique collision of Indian and Eurasian plates and comprises several transform faults (Farah et al. 1979; Farah and DeJong 1984; Jadoon et al. 1994, 1992; Jadoon and Khurshid 1996; Lawrence et al. 1981; Yeats and Lawrence 1982). The southern section comprises the southwest-oriented Bela–Chaman–Kurram belt, which connects the Indian plate to the Eurasian
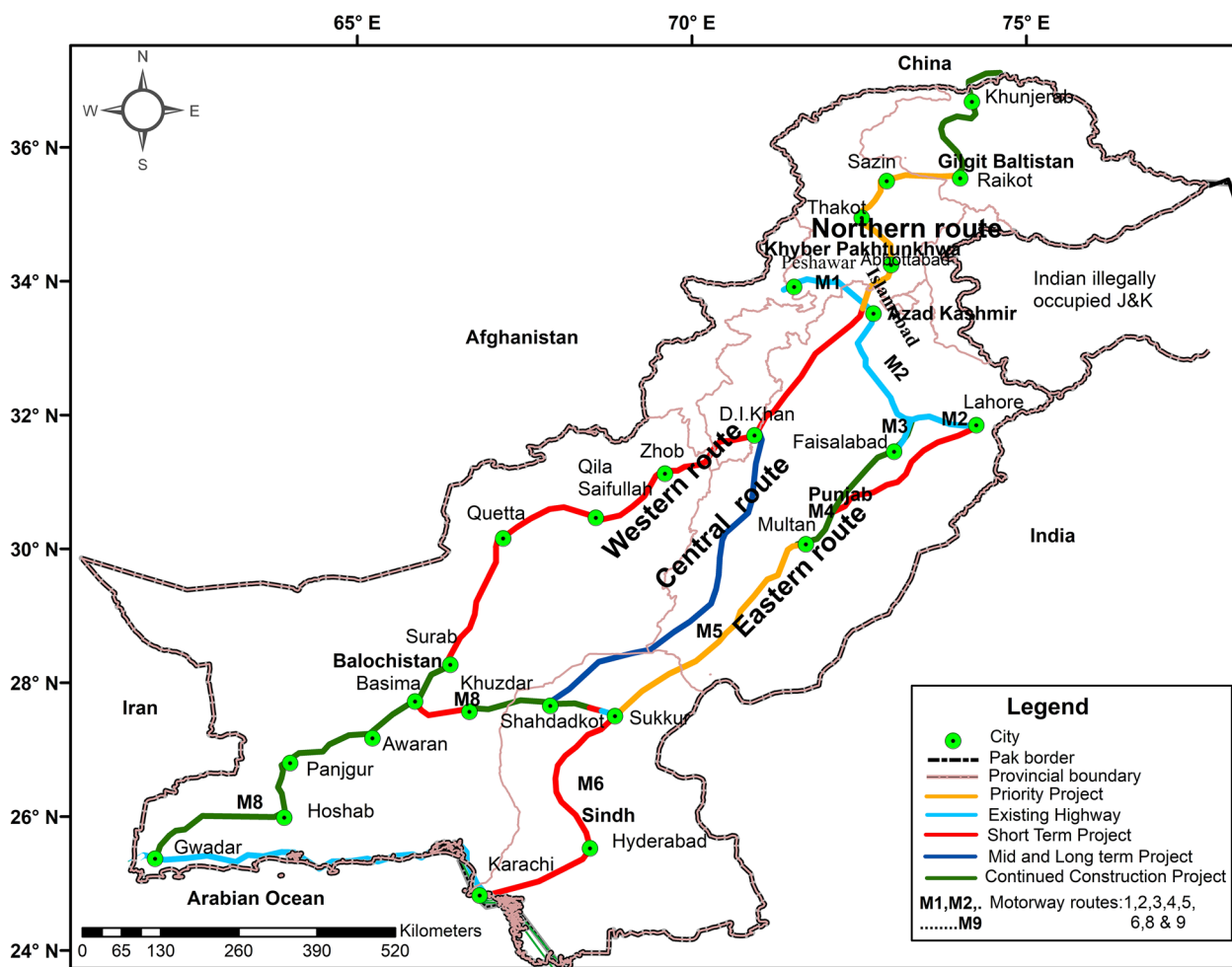

Fig. 2 Map of the China–Pakistan Economic Corridor (CPEC) routes project in Pakistan, from its initiation in 2013 to its projected completion in 2030 (source www.cpec.gov.pk). The CPEC routes connect China's western region of Xinjiang to Pakistan's southwestern port of Gwadar, passing through various regions and cities of Pakistan

plate. Along the western boundary of the Indian plate, the Arabian Ocean's Murray ridge and Owen-fracture zone are generated by the interaction of the three plates (Eurasian–Arabian–Indian). On the south coast of Pakistan, the Makran subduction zone is formed as a result of the interaction of the Arabian and Eurasian plates next to the deep port of Gwadar (Malkani and Mahmood 2016). Figure 1 shows CPEC routes with major tectonic elements and the number of well-known recognized faults in Pakistan. The Himalayas, Pamir-Hindukush, Karakoram, Sargodha high, Suleiman mountains, Run of Kutch, and Makran area are the most vulnerable seismic zones in the world (Waseem et al. 2020). The following methods have been chosen for the hazard computation of CPEC routes.

3 Methods

This study is carried out by taking into account the mainshock events delineated by coordinates 58°–83° N and 22°–40° E and by setting up a 15-km fishnet grid in ArcGIS software (Fan et al. 2022) on either side of the CPEC routes, which run from Khunjerab to Gwadar in Pakistan. Furthermore, the updated seismic source model of Pakistan developed by Waseem et al. 2020 is used. The Gardner and Knopoff (1974) algorithm (Gardner and Knopoff 1974) is used to de-cluster the homogenized earthquake catalogue (25AD-2020) in Zmap (ver. 6.0) software by using the MATLAB R2013a platform. The Open Quake engine, version 3.10, is used to compute the seismic hazard. The source model, GMPEs, and ground motion intensity parameters are used as input parameters. The source model includes the vertices of each seismic source zone, as well as a description of the tectonic regime, a-value and b-value, maximum and lowest threshold magnitude, and upper and lower seismic focal depth encountered in each seismic source zone. The choice of mean (50%) and mean plus one standard deviation (84th percentile) has due significance in the determination of the focal depths of respective seismic source zones. However, the 84th percentile is opted due to the reason; ground motion hazard is abnormally higher due to the outdated choice of using the mean (50%). The four updated ground motion prediction equations are assigned to distinct tectonic regimes (i.e., active shallow crust, subduction interface, and intraslab), and equal weights are assigned to each GMPE on the logic tree.

The traditional PSHA areal source initially computes hazard curves for various ground motion and spectral acceleration intensities at designated areas of interest. The hazard maps can then be interpolated at 10% and 2% probability of exceedance in 50 years. The Open Quake engine uses Eq. (1) to determine the rate of earthquakes.

$$R_{(b)} = \sum v_i \iint P[B > b/m, r] f_{m(M)} \cdot f_{R/M}(r, m) d_r d_m \tag{1}$$

whereas $R_{(b)}$—the annual rate of earthquakes fabricating earthquake amplitude "B" greater than "b", v_i is the annual rate of earthquakes in a seismic source greater than the minimum threshold magnitude.

$P[B > b/m, r]$ is the probability that an earthquake at a particular location, at distance "r" with magnitude "m" produces an amplitude "B" [e.g., peak ground velocity (PGV), peak ground displacement (PGD), PGA, etc.] greater than "b"; $f_{m(M)} \cdot f_{R/M}$ are the probability density functions for earthquake distance and magnitude.

The annual rate of earthquakes given by the equation can be strained over all the seismic sources by summation. The earthquake occurrence process is Poissonian, and based on this assumption, Eq. (2) estimates the probability that ground motion "B" will exceed "b".

$$P[B > b/m, r] = 1 - e^{R_{(b)}} \tag{2}$$

The methods include the collection and compilation of earthquake data catalogs; data homogenization to a single magnitude scale; declustering, completeness analysis; geological development of seismic source models; source characterization; determination of Guttenberg–Richter (G–R) parameters of seismic source zones; selection of GMPEs; and epistemic uncertainty of the computations by incorporating a logic tree.

3.1 Data processing for the earthquake catalogue

The first step in predicting the probability of seismic hazard in a zone of interest is to compile an accurate, up-to-date, and homogenized earthquake catalogue. A reliable catalog records all earthquakes that occur in the region and must be homogenized on a single magnitude scale. It is used to compute seismic zone activity rates and to identify the seismic source model. The composite and homogenized strong motion data compiled by Khan et al. (2018) for Pakistan from 25AD-2016 are used in this study (Khan et al. 2018). The earthquake catalogue was further updated for the years 2017–2020 by including data from several online sources, such as the International Seismological Centre, the United States Geological Survey, and local networks demarcated by coordinates 58°–83° N and 22°–40° E. The data from these sources are recorded on a variety of magnitude scales, including surface–wave magnitude (M_s), local magnitude (M_L), body-wave magnitude (m_b), and moment magnitude (M_w). The data are then homogenized to the moment magnitude scale using Zara et al. (2014) relationships, which were validated by Khan et al. (2018) for this region.

For the conversion, the bilinear Eqs. (3), (4), (5), and (6) are employed. For the conversion of M_s to M_w, bilinear Eqs. (3) and (4) are used,

$$M_w = 0.58 \times M_s + 2.46 \tag{3}$$

For $3.5 \leq M_s \leq 6.0$

$$M_w = 0.94 \times M_s + 0.36 \tag{4}$$

For $6.1 < M_s \leq 8.2$

For the conversion of M_b to M_w, bilinear [Eq. (5)] is used,

$$M_w = 0.93 \times M_b + 0.45 \tag{5}$$

For $4.0 \leq M_b \leq 6.2$

For conversion of M_L to M_w [Eq. (6)], (Zare et al. 2014) is used,

$$M_w = 1.01 \times M_L - 0.05 \tag{6}$$

For $4.0 \leq M_L \leq 8.3$

The different magnitude scale data are converted to the moment magnitude scale for the reason that the newest GMPEs utilize the moment magnitude as the analytical variable. The complete earthquake catalog included 33,210 events with moment magnitudes greater than 4.0 from 25 AD to 2020.

3.2 Declustering

To avoid the overestimation of hazard analysis, the declustering technique is used, which separates dependent events (foreshocks and aftershocks) from independent events (the main shock). The Poissonian assumption is used to calculate the probability of a hazard recurrence, which takes into account the separate events that occur arbitrarily in time and space. The dependent events are spatially and temporally dependent on the independent events. The Gardner and Knopoff (1974) approach is used in the ZMAP 6.0 package (Wiemer 2001) on the MATLAB R2013a platform to remove the dependent events (Wiemer 2001). The approach was developed for the Southern California region, but it is also applicable to other parts of the world with similar tectonic settings. This algorithm has been used in several studies in Pakistan, e.g., Building code of Pakistan (2007), Zaman et al. (2012), Waseem et al. (2018), and Mahmood et al. (2020).

Using Gardner and Knopoff's (1974) technique, in the declustered earthquake catalogue, a total of 6637 independent events were found that corresponded to the respective defined seismic source zones. To delineate the source model, a focal depth of 50 km is used as a dividing line in the model to separate shallow and deep-focus earthquakes. The catalogue includes 5506 shallow and 1131 deep-focus earthquake events. Figure 3 shows the deep-focus earthquakes (focal depth > 50 km) that are mainly concentrated in the northern and lower western CPEC routes, and shallow-focus earthquakes (focal depth < 50 km) are mainly concentrated in the northern, central, and western CPEC routes.

3.3 Completeness analysis

The recurrence relationships used to calculate the annual activity rate of earthquakes are based on the completeness periods of earthquake magnitudes. The Tinti and Mulgaria (1985) procedure is used to perform the completeness analysis of the de-clustered, homogenized earthquake catalogue. To perform the completeness analysis, all independent events were grouped into 0.5 unit of magnitude bins (e.g., 4.00–4.50, 4.51–5.00, 5.01–5.5, 5.51–6.00, 6.01–6.50, 6.51–7.00, 7.01–7.50, and 7.51–8.00). Every magnitude range is subjected to a completeness check, and the completeness years are determined so that the data in the completeness periods can be considered to compute the activity rate in each source zone. The year 1902 was a completeness period of earthquakes for the 7.51–8.00 magnitude range, and this period is from 1902 to 2020. Because the data prior to 1902 were insufficient and would have led to an underestimation of activity rates, only the earthquakes that occurred during the completeness periods were used. The total number of events was then plotted against the years on a graph, and the best fit line was drawn across the data points to determine the completeness period (Table 1). Figure 4 shows the completeness periods of earthquake moment magnitudes.

3.4 Geological development of seismic source model

The classical Cornell (1968) approach requires a seismic source model as an input parameter for the computation of hazard analysis. As shown in Fig. 5, a modified areal seismic source model developed by Waseem et al. (2020) for Pakistan is used in this study. An aerial source model signifies the spatial distribution of seismicity patterns in areas with unknown fault locations (Sesetyan et al. 2018b). In Pakistan, faults are not very well constrained in terms of slip rates, dip angles, rupture, geometry, and other parameters. Therefore, in the absence of well-marked faults in the region, area source zones have been used in the current study. Faults do, in fact, show the variation of real seismic hazard, but due to the limitations on fault data, they were not used. Area sources are defined based on the fault trends and by using local geologic information. The used areal model describes the probable seismic source zones based on tectonics,
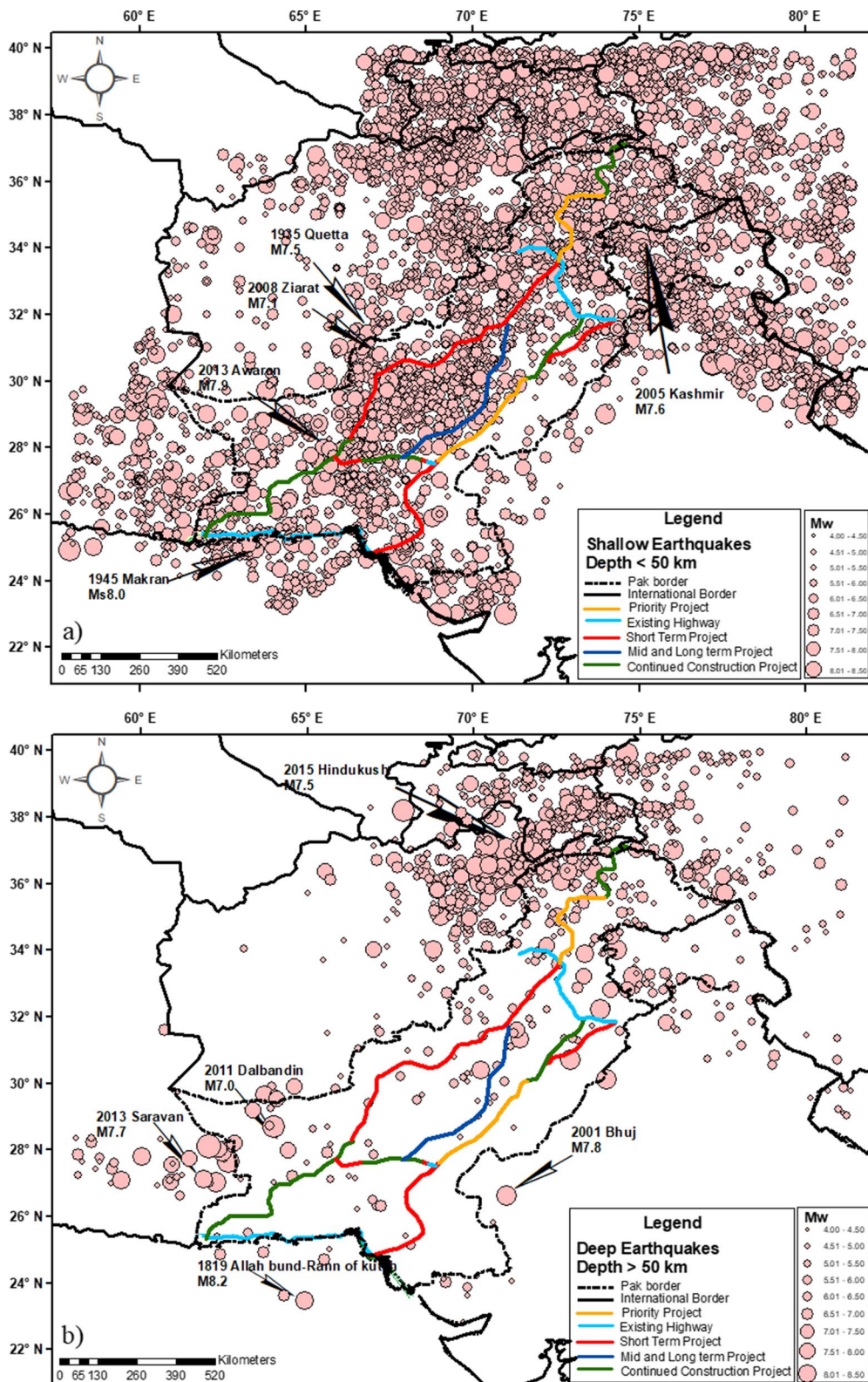
Fig. 3 The earthquake catalogue utilized for probabilistic seismic hazard analysis (PSHA) computation of China–Pakistan Economic Corridor (CPEC) routes in Pakistan, **a** earthquake events with focal depth up to 50 km **b** earthquake events with focal depth greater than 50 km

Table 1 The completeness periods of the seismic catalogue, which indicate the moment magnitude ranges of 0.5 units above the minimum threshold moment magnitude of 4.0, and the duration of time for which the catalogue is considered to be complete

Moment magnitude (Mw) ranges	Completeness period
4.00–4.50	1999–2020
4.51–5.00	1980–2020
5.01–5.50	1978–2020
5.51–6.00	1977–2020
6.01–6.50	1969–2020
6.51–7.00	1962–2020
7.01–7.50	1906–2020
7.51–8.00	1902–2020
8.01–8.50	1902–2020

active fault zones, and seismicity patterns. The modified source model includes the 34 active shallow crust seismic source zones, four deep subduction intra-slab seismic source zones, and one deep subduction interface seismic source zone. Active shallow seismic source zones are associated with seismicity up to a focal depth of 50 km, whereas deep subduction source zones are associated with seismicity greater than a focal depth of 50 km. As shown in Fig. 6a, b, the shallow and deep seismic source models with CPEC routes are established separately with a borderline focal depth of 50 km. In the modified seismotectonic model, deep seismic source zones overlapped with shallow active source zones. Each seismic source zone (SSZ) boundary and shape must be defined by the knowledge decree. The seismically high and low zones can be differentiated based on well-defined active faults. Whereas the region lacks marked active faults, the seismicity pattern of each SSZ and geologic expert opinion is employed to demarcate each deep SSZ. In this model, the geological information of the region is prioritized over seismicity information to distinguish adjacent SSZ. The Karakoram ranges, for example, were separated from the Hindukush ranges, while the Himalayan region is separated from the Kohistan Island arc sequence. The seismic source model presented in this work also considers the known active faults in Pakistan and adjacent regions (Waseem et al. 2020). However, the seismic source zones were identified by taking into account the region's tectonic features, and a summary of noticeable tectonic features is provided in the following section (Fig. 1).

The geology and tectonics of North Pakistan are characterized by the coexistence of three terranes: (1) the Karakoram block (SSZ 2, 3); (2) the Kohistan Island Arc (SSZ 5); and (3) the Indian Plate (SSZ 9, 10, 13) (Searle et al. 1999). The Karakoram block is separated from

Kohistan Island Arc to the south by the Main Karakoram Thrust. In the north and south, the Kohistan Island Arc is confined to the Main Karakoram Thrust and Main Mantle Thrust. The Indian Plate lies south of the Main Mantle Thrust. The KB contains sedimentary rocks (Paleozoic–Mesozoic) in its northern wedge, Karakoram batholith rocks (Cretaceous-Miocene) in its central wedge, and a metamorphic complex (late Paleozoic-Cenozoic) in its southern wedge. In this part, the rocks are highly deformed due to the pre- and post-Indian-Eurasian collision with granitic intrusions of the Eocene-Miocene age (Zanchi and Gaetani 2011). The Karakoram block has overall low seismicity, as evidenced by a M_w 6.0 Gilgit earthquake, but the rocks at high elevations have residual strength due to active tectonics and several collisional episodes of the India–Asia collision (Rehman et al. 2021). Even the low moment magnitude value in the region can cause catastrophic hazards to infrastructure. The KB has several faults, including but not limited to the Karakoram fault system, North Pamir fault, South Pamir fault, Tirch Mir fault, and Reshun fault. The area has high induced seismicity in the north and northwest regions due to the presence of the Pamir-Karakoram (SSZ 2, 29) and Hindukush ranges (SSZ 1,32,33) (Waseem et al. 2018). The KIA has metasedimentary and volcanic rocks (Cretaceous–Paleocene) in the north, along with Main Karakoram Thrust: the Kohistan batholith (late Cretaceous) and Lahor granite intrusion in the center, and mafic–ultramafic complexes (Early Cretaceous) in the south, along the Indus suture zone (Jagoutz and Schmidt 2012; Petterson 2010). The Pamir and Hindukush mountains stretch along this arc and have experienced shallow-intermediate focus earthquakes (Mukhopadhyay and Dasgupta 2015). The Nanga Parbat syntaxial (SSZ 6) bend in the Kohistan Island Arc is rising at a rate of 6 mm/yr., indicating active tectonics in the region (Treloar et al. 1991). The Ladakh arc is the eastern extension of Kohistan Island Arc. Based on the cross-cut connection of Jutal dykes in the collisional regime, the Kohistan Island Arc is believed to have collided with Karakoram block around 75 Ma in the Late Cretaceous (Searle et al. 1999). Around 50–55 Ma ago, the Indian plate collided with the Kohistan Ladakh arc (Bignold and Treloar 2003; Petterson and Windley 1985; Rehman et al. 2011).

The Himalayas and Hazara Kashmir syntaxis (HKS) (SSZ 10) were formed due to the collision of the Indian and the Eurasian plate around 50–55 Ma ago (Ding et al. 2016). In Pakistan, the Indian plate Himalayan sequence south of the Indus suture zone may be divided into three tectonostratigraphic divisions: (1) the Greater Himalaya; (2) the Lesser Himalaya; and (3) the Sub-Himalaya (Qasim et al. 2018). The Greater
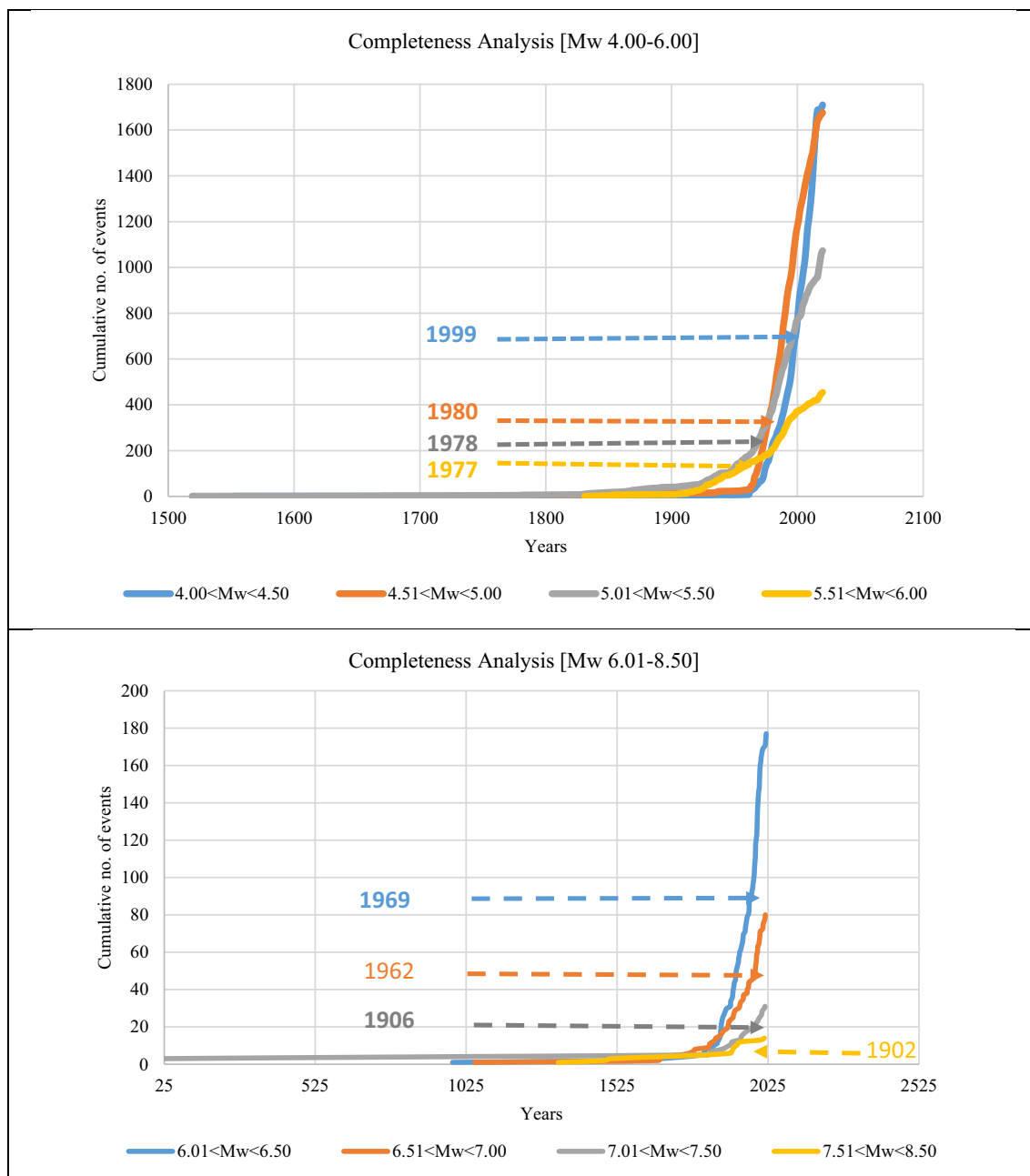
Fig. 4 Completeness periods obtained through regression analysis using the Tinti and Mulargia (1985) method for CPEC routes in Pakistan by considering the moment magnitude range of 0.5 units above the minimum threshold moment magnitude of 4.0

Himalayas are comprehended to the north of Main Central Thrust (MCT). The MCT's position in Pakistan is disputed; nevertheless, Chaudhary and Ghazanfar (1990) suggested the Batal fault that passes through the Kaghan valley is equivalent to the MCT. In the north and south, the Lesser Himalayas are surrounded by the MCT and main boundary thrust (MBT), respectively (Chaudhry and Ghazanfar 1990). The region has high

seismicity due to the presence of anticlinorium HKS and several active faults, including the sinistral Jhelum fault, Nathiagali thrust (NT), and Panjal thrust (PT). In the north and south, the Sub-Himalayas (SSZ 15) are limited by the Himalayan frontal thrust (HFT) and the MBT. The major active faults include the dextral Kalabagh fault (KB), the Riasi Thrust (RT), and the Salt Range Thrust (SRT). The zone primarily consists
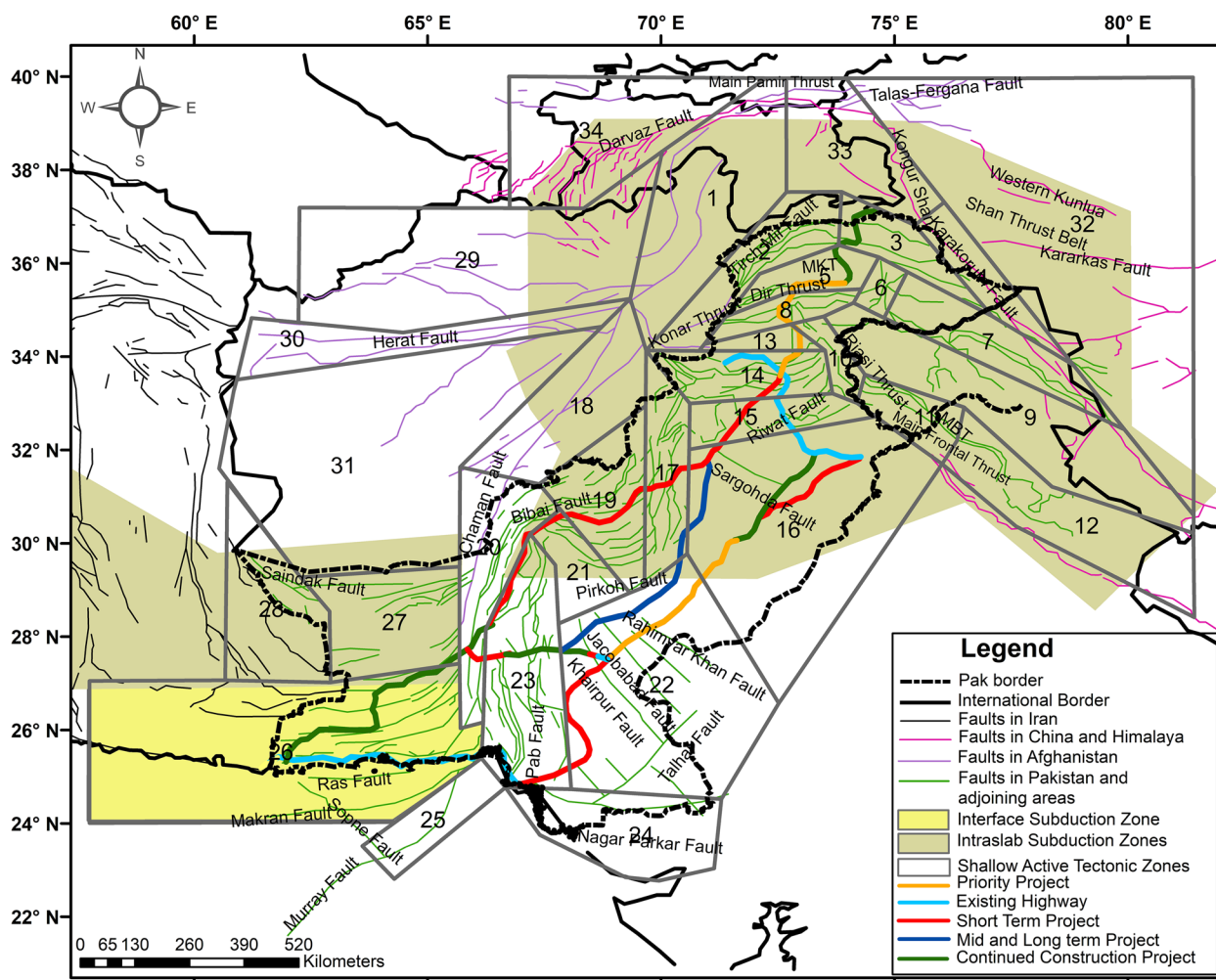
Fig. 5 The seismic source model that is used for the hazard analysis of the China–Pakistan Economic Corridor (CPEC) routes in Pakistan (Modified after Waseem et al. 2020). The model provides a representation of the potential interface subduction zone, intraslab subduction zone and shallow active tectonic zone along the CPEC routes in Pakistan

of Cenozoic rocks with limited exposure to Cambrian layers.

The Indian plate platform, which represents the stable continental shelf, is separated into two tectonic zones: (1) the Indian shield zone (Nagar Parkar ridge) (SSZ 24) and (2) the Indus platform tectonic zone (SSZ 16). The Indian–Eurasian collision produced reverse faults as a result of the compression (Chaudhry and Ghazanfar 1990). The presence of Jacobabad and Kandkot highs, the Sukhar rift, and the Nagar Parkar ridge have resulted in high seismicity in the region. Major earthquakes include 893 Shahbandar (M_w 8.0), 980 Mansura (M_w 6.0), 1668 Samawani (M_w 6.5), 1819 Allah bund (M_w 7.7) and 2001 Bhuj (M_w 7.9). The Indus trough and plains, on the other hand, have diffused seismicity compared to the Indian shield zone, possibly because of less active faults.

The late Cretaceous–Neogene India–Eurasia collision deformed the western boundary of the Indian plate, which is marked by the Bela-ophiolite mélange zone (SSZ 23) (Zaigham and Mallick 2000). The Chaman Ornach-Nal transform fault zone (SSZ 20), which is composed of the Bela ophiolite belt, separates the Indian plate in the east from the Makran Chagai trench of the Eurasian plate in the west (Lawrence et al. 1981). The Kirthar range is surrounded to the east by the Jacobabad Khairpur high (SSZ 22) and the Indus platform. Pakistan's central and southern regions are divided into four major tectonic provinces: (1) the Bela Chaman Kurram fault zone and ophiolite belt/Axial belt (SSZ 17, 23); (2) the Indian plate platform (SSZ 16); (3) the Chagai Makran trench arc system (SSZ 26, 27, 28); and (4) the Indian Ocean (SSZ 25, 26).
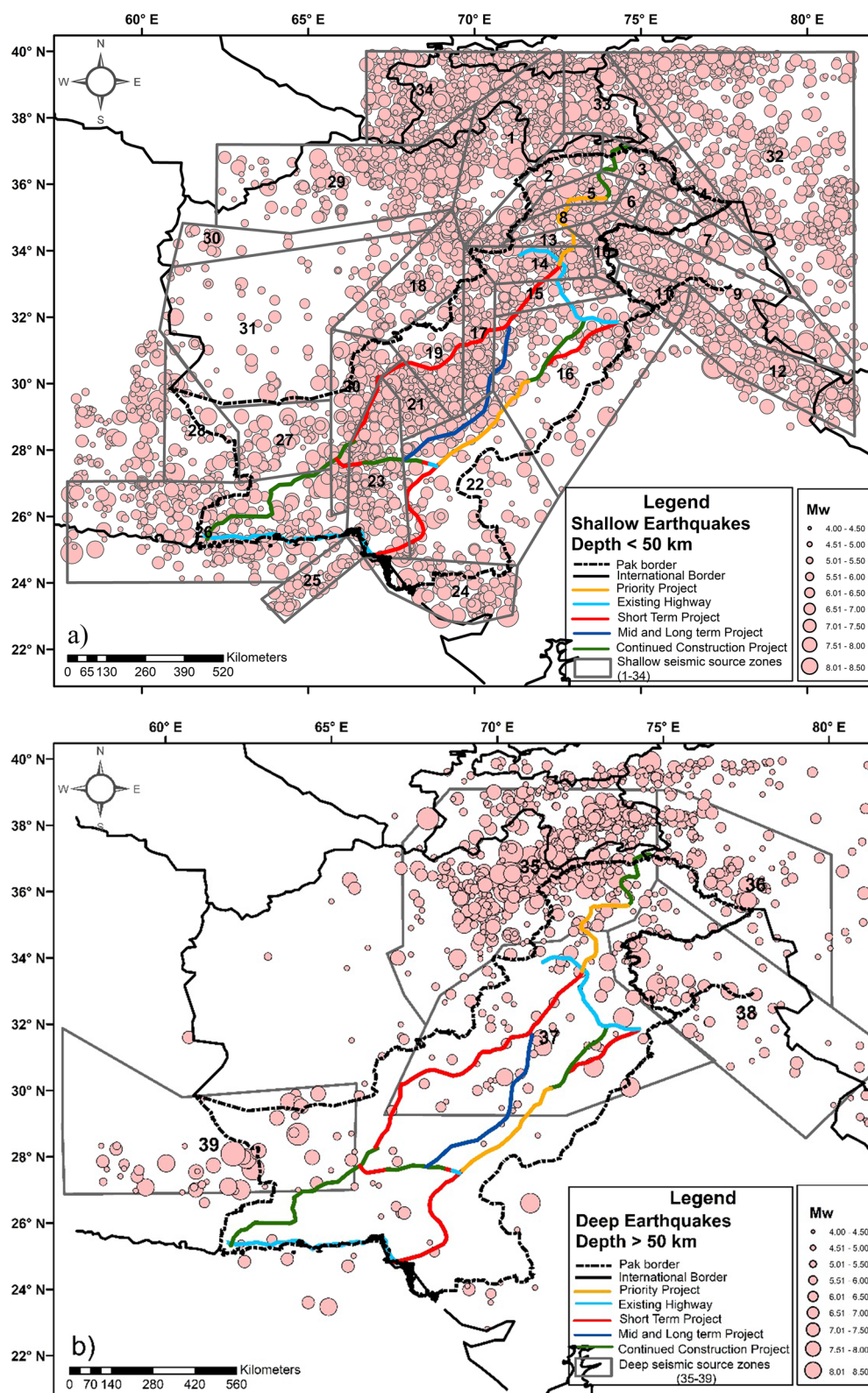
Fig. 6 The individual shallow active and deep interface/intraslab seismic source models used for CPEC (China–Pakistan Economic Corridor) routes in Pakistan. **a** The shallow active source model takes into account shallow earthquake events encountered within the uppermost 50 km of the Earth's crust **b** the deep interface/intraslab seismic source model considers deep earthquake events encountered at depths greater than 50 km

The ophiolite axial belt is divided into the Suleiman range, Sibi Syntaxis, Kirthar range, Bela-ophiolite mélange zone, and Ornach-Nal fault zone. The Suleiman Range (SSZ 19) is a fold and thrust belt formed by the Indian plate rotating clockwise and colliding with the Eurasian plate. Because of active tectonics and the presence of the Kingri, Waziristan-Loralai, and Muslim Bagh faults, the area has high seismicity. In the region, intermediate and shallow-focus earthquakes are common. Waseem et al. (2019) have found this range to have the highest seismic hazard potential. Sibi syntaxis (SSZ 21) represents the foreland syntaxial bend with dextral transpression and basement faults. Kachhi (1909) and Sharig (1931) recorded high induced seismicity in earthquakes of M_w 7.1 and 6.8, respectively. The Kirthar range (SSZ 23) is a north–south-oriented external foreland thrust fold belt contained by passive roof duplex transpression. The Kirthar fault separates the Kirthar and Khude fold belts. The zone was hit by the 1931 Mach earthquake (Mw 7.3). The Bela ophiolite mélange (SSZ 23), a suture zone, represents the internal thrust and fold belt with sinistral transpression. The zone is bounded to the east by faults including the Diwani, Mor, and Pab faults, and to the west by the sinistral strike-slip Ornach-Nal fault zone. This fault is further interpolated and marks the Makran subduction zone (SSZ 26) boundary in the Indian Ocean. The zone contains the faults, including Chaman, Ghaziabad, and Ornach-Nal faults. Based on InSAR data, the slip rate of the Ghazaband fault is 16.3 + 2.3 mm/yr (Fattahi and Amelung 2016). The active sinistral Chaman fault (SSZ 20), with a length of more than 850 km, forms a transpressional border between the Eurasian and Indian plates in the northwest of Pakistan and extends into Afghanistan, joining the dextral Herat fault (SSZ 30,31) and the Pamir fault system (MKT in Pakistan) (Lawrence et al. 1981). Based on InSAR data, the slip rate of the Chaman fault is 8 + 3.1 mm/yr (Fattahi and Amelung 2016). The induced high seismicity in the zone is described by the 1935 Quetta earthquake (M_w 7.6). The Chagai–Makran trench arc system is subdivided into two tectonic blocks, namely (i) the Ras Koh-Chagai arc (SSZ 27) and (ii) the Makran flysch basin (SSZ 26). The Chagai and Mashkhel in the Sistan region represent the tectonic setting of the Island Arc and Forearc, with deep subduction megathrusts in the trench. The area contains the Dalbandin and Ras Koh faults, in addition to several unidentified faults. The major earthquakes in this block include the 2011 Dalbandin earthquake (M_w 7.2) and the 1983 Iran earthquakes (M_w 7.0).

The Makran flysch basin is divided into two tectonic zones: (i) Central Makran and (ii) the Makran coastal trough. The Central Makran zone has intermediate subduction megathrusts represented by the Panjgur and Hoshab Faults, which induced the 1929 earthquake (M_w 6.5). The faults such as Ormara, Makran Coast faults, and Makran subduction thrust faults all mark shallow subduction megathrusts in the Makran Coastal Trough zone (SSZ 26). The induced high seismicity of this active tectonic zone is characterized by the 1945 Markran earthquake (tsunami) (M_w 8.2) and the 2013 Awaran earthquake (M_w 7.7). The Darvaz fault zone (the Pamirs) is considered as SSZ 34. Deep seismicity (focal depth > 50 km) is concentrated mostly in Pakistan's Himalaya–Hindukush–Karakoram mountainous area, demarcated by zones (SSZ 35,36,37,38) and the Makran subduction zone (SSZ 39) (Fig. 6b).

3.5 Source characterization

The seismic source zones are characterized by identifying maximum magnitude potential, the earthquake count, and the G–R parameters (Gutenberg and Richter 1956) in each source zone. The maximum magnitude potential of each SSZ is computed as: (1) by finding the maximum magnitude value encountered in each source zone with the addition of 0.5 units to handle the probable estimation errors or (2) by taking the fault-based magnitude potential of the source zones. Waseem at el. (2020) have shown that both methods produce magnitudes in a similar series. As a result, the maximum historic earthquakes approach is used to calculate the maximum magnitude potential of seismic source zones with an addition of 0.5 units to the highest observed moment magnitude value of each source zone. The key advantage of using this approach is that it does not abnormally reduce the hazard level.

3.6 Gutenberg–Richter (G–R) parameters of seismic source zones

After completeness analysis, a declustered earthquake catalogue and earthquake count of each seismic source zone are utilized to calculate the G–R parameters of each SSZ following the G–R recurrence law (Gutenberg and Richter 1956). It is attained for all defined source zones by the execution of least square regression analysis on the logarithm of the cumulative number of earthquakes and their respective moment magnitude values in each source zone. The standard G–R recurrence law accommodates an infinite number of earthquake magnitudes (Kramer 1996). As a result, the truncated G–R recurrence law is employed to predict the anticipated activity rate in each source zone. Equation (7) gives the truncated law formula:

$$\lambda = v_0 \cdot \frac{\exp^{-\beta \cdot (M_w - M_w^{\min})}}{1 - \exp^{-\beta \cdot (M_w^{\max} - M_w^{\min})}} \quad (7)$$

whereas $v_0 = \exp(\alpha - \beta \cdot M_w^{\inf})$ λ=activity rate, $M_w^{\max}$ and $M_w^{\min}$—the maximum and minimum moment magnitude bounds of the source. The G–R parameters are

a, *b*, *α*, and *β*. However, $\alpha = 2.303^*a$ and $\beta = 2.303^*b$. The *a*-value suggests the cumulative seismicity of each zone. The *b*-value is a ratio of large to small magnitudes, and a value around 1 indicates a seismically active zone. A lower *b*-value indicates a higher potential for major future earthquakes and vice versa.

Table 2 The table presents the characterization of seismic source zones based on the geological, tectonic, and seismological data, including the location, area, maximum magnitude, seismicity rate, and recurrence intervals of earthquakes

Seismic source zone (SSZ)	No. of events (N)	*a* value	*b* value	*λ* value	*α* value	*β* value	v_o	M_{min}	M_1	M_{max}
1	266	4.401	0.800	15.853	10.137	1.843	15.860	4.0	7.3	7.8
2	77	3.907	0.794	5.388	8.999	1.828	5.389	4.0	7.4	7.9
3	53	4.503	0.953	4.869	10.370	2.196	4.869	4.0	6.4	6.9
4	47	2.822	0.631	1.973	6.500	1.455	1.973	4.0	7.5	8.0
5	37	2.529	0.5814	1.600	5.825	1.338	1.599	4.0	7.4	7.9
6	13	2.270	0.621	0.611	5.228	1.430	0.611	4.0	6.4	6.9
7	51	3.974	0.850	3.720	9.152	1.959	3.720	4.0	6.7	7.2
8	37	2.999	0.685	1.808	6.907	1.578	1.808	4.0	6.9	7.4
9	165	4.585	0.884	11.117	10.560	2.037	11.122	4.0	8.5	9.0
10	33	3.041	0.733	1.285	7.004	1.688	1.285	4.0	7.5	8.0
11	47	3.557	0.767	3.070	8.193	1.768	3.070	4.0	7.7	8.2
12	166	4.361	0.830	10.952	10.044	1.912	10.956	4.0	7.1	7.6
13	10	2.953	0.814	0.495	6.802	1.876	0.495	4.0	5.7	6.2
14	86	4.283	0.865	6.618	9.864	1.993	6.619	4.0	7.5	8.0
15	61	4.309	0.912	4.544	9.923	2.102	4.544	4.0	6.6	7.1
16	144	4.567	0.896	9.621	10.519	2.063	9.624	4.0	7.1	7.6
17	101	5.078	1.035	8.672	11.695	2.383	8.674	4.0	7.0	7.5
18	71	4.330	0.894	5.645	9.973	2.060	5.647	4.0	7.7	8.2
19	74	5.721	1.196	8.646	13.175	2.754	8.649	4.0	6.8	7.3
20	95	3.921	0.789	5.826	9.031	1.817	5.828	4.0	7.7	8.2
21	73	4.210	0.882	4.786	9.697	2.032	4.787	4.0	7.5	8.0
22	88	3.065	0.611	4.18	7.059	1.407	4.181	4.0	6.4	6.9
23	157	5.455	1.085	13.026	12.563	2.498	13.031	4.0	8.2	8.7
24	46	3.231	0.727	2.091	7.441	1.675	2.091	4.0	7.8	8.3
25	33	3.978	0.854	3.65	9.162	1.966	3.650	4.0	6.1	6.6
26	204	2.191	0.668	0.33	5.047	1.539	0.329	4.0	8.2	8.7
27	47	3.973	0.846	3.886	9.151	1.948	3.886	4.0	6.6	7.1
28	45	2.969	0.668	1.978	6.839	1.539	1.978	4.0	6.8	7.3
29	252	4.594	0.835	17.931	10.580	1.923	17.940	4.0	7.0	7.5
30	25	3.378	0.806	1.427	7.781	1.856	1.427	4.0	7.5	8.0
31	45	3.860	0.852	2.834	8.890	1.962	2.834	4.0	7.0	7.5
32	542	5.667	0.998	47.195	13.051	2.299	47.228	4.0	7.7	8.2
33	137	4.486	0.856	11.442	10.331	1.973	11.446	4.0	7.6	8.1
34	249	4.924	0.915	18.256	11.340	2.108	18.265	4.0	7.3	7.8
35	391	4.114	0.703	19.911	9.475	1.620	19.922	4.0	7.9	8.4
36	81	4.546	0.957	5.214	10.470	2.204	5.215	4.0	7.5	8.0
37	36	2.699	0.620	1.65	6.217	1.429	1.649	4.0	7.4	7.9
38	38	3.302	0.747	2.062	7.605	1.720	2.061	4.0	7.7	8.2
39	36	2.820	0.631	1.972	6.494	1.453	1.972	4.0	7.5	8.0

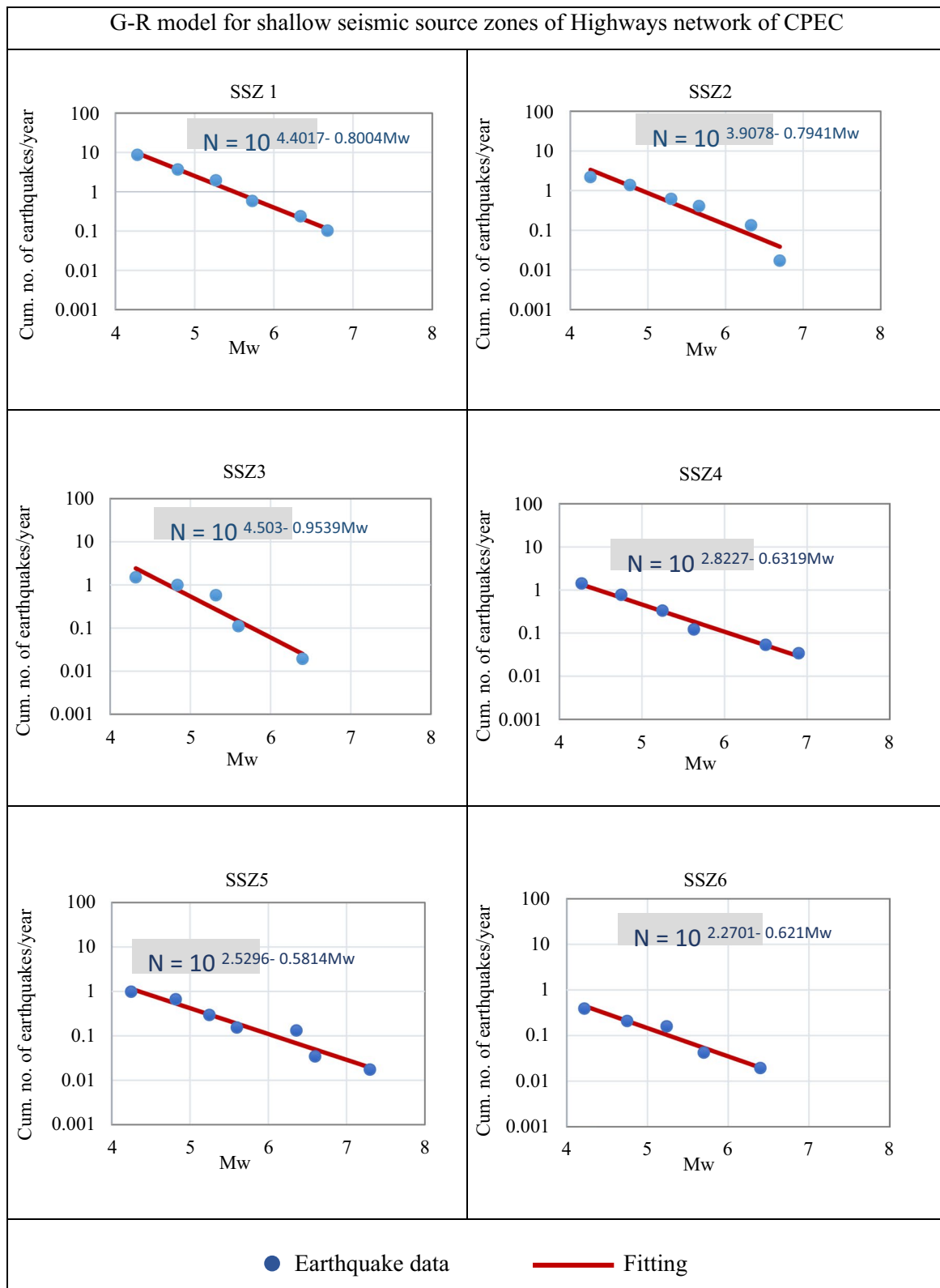$M_{max} = M_1$ (maximum observed magnitude in each source zone) + 0.5 units

Fig. 7 The Gutenberg–Richter model plots, illustrating the expected earthquake magnitude for seismic source zones (1–39) in Pakistan. The model is based on historical seismic data and can be used to estimate the probability of an earthquake of a certain magnitude occurring in a specific source zone
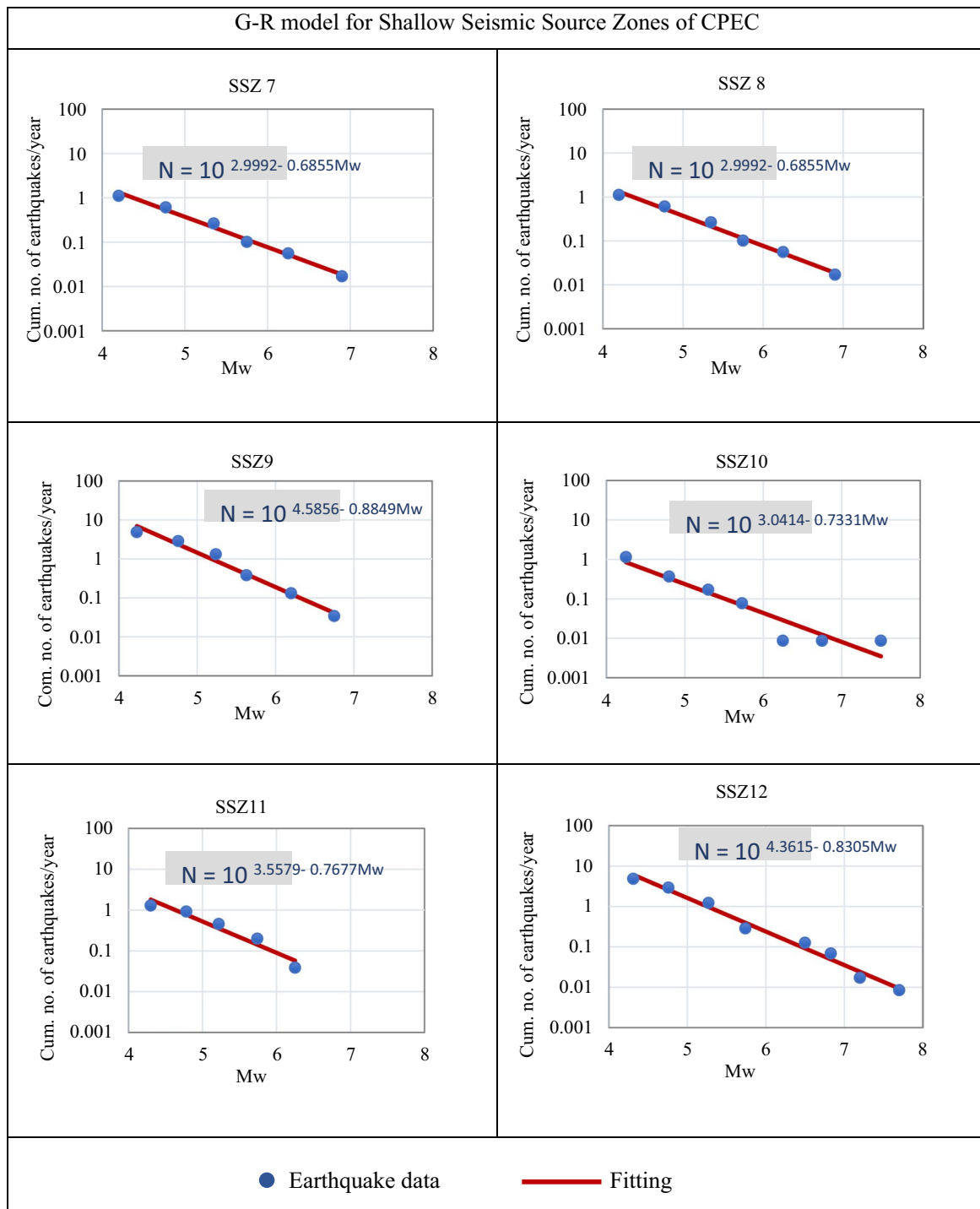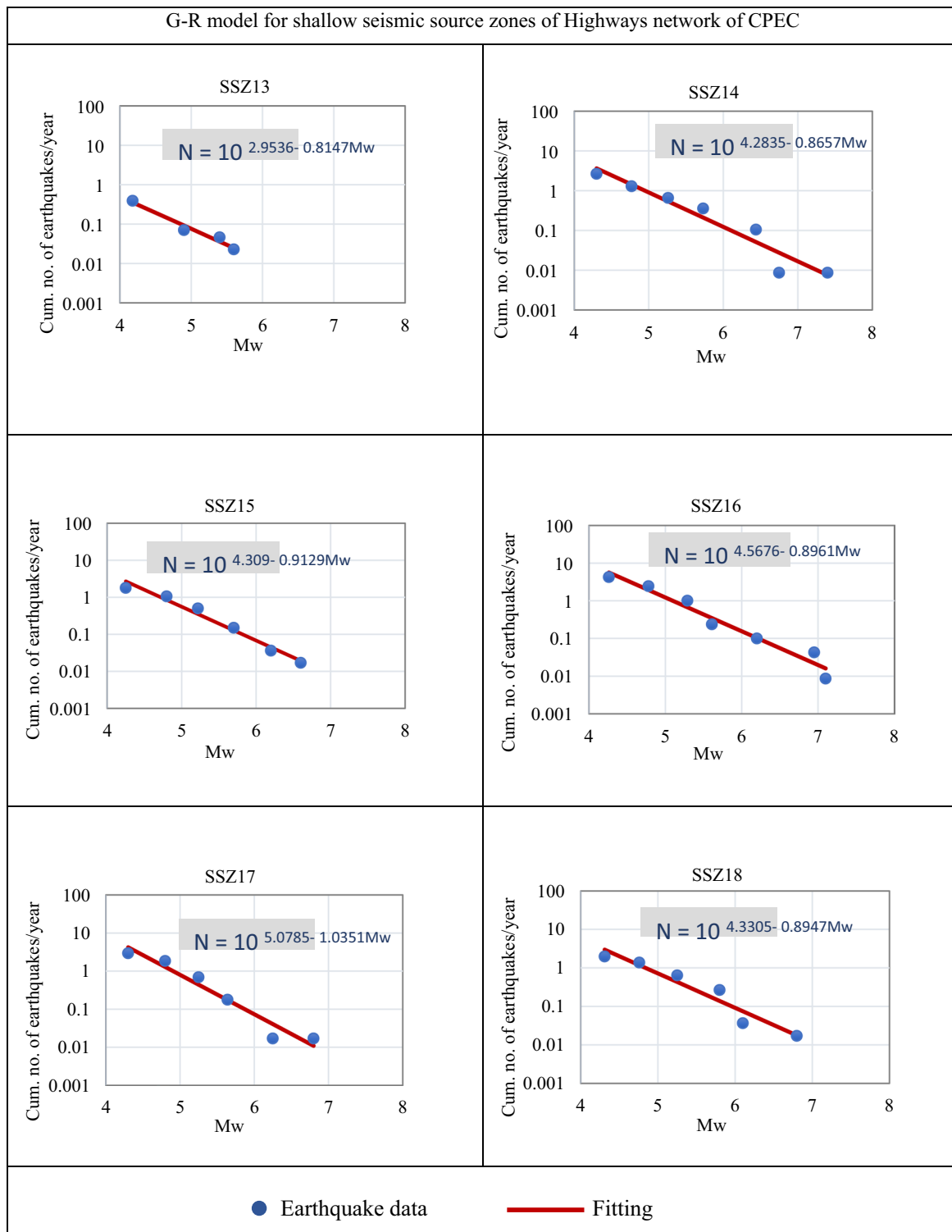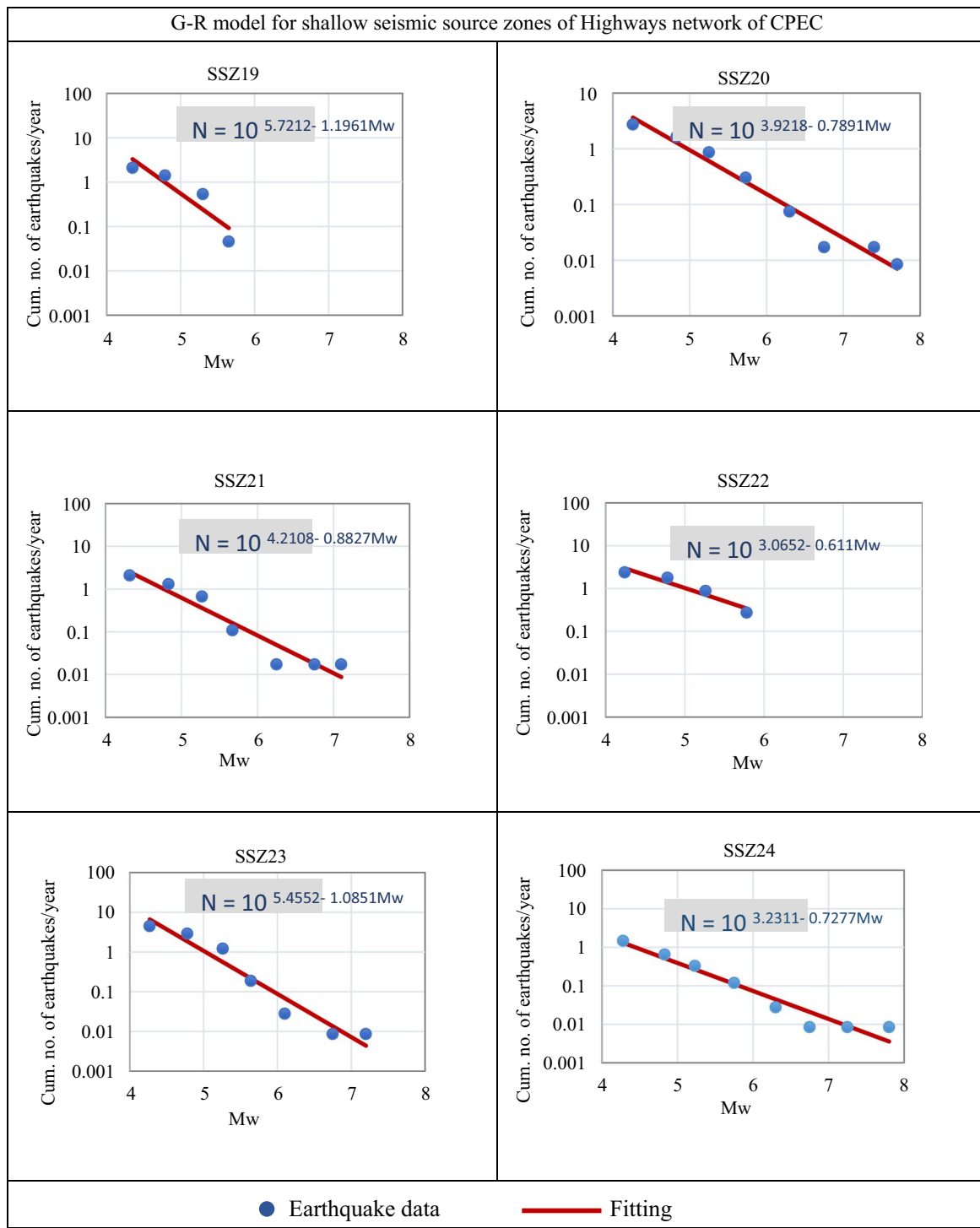
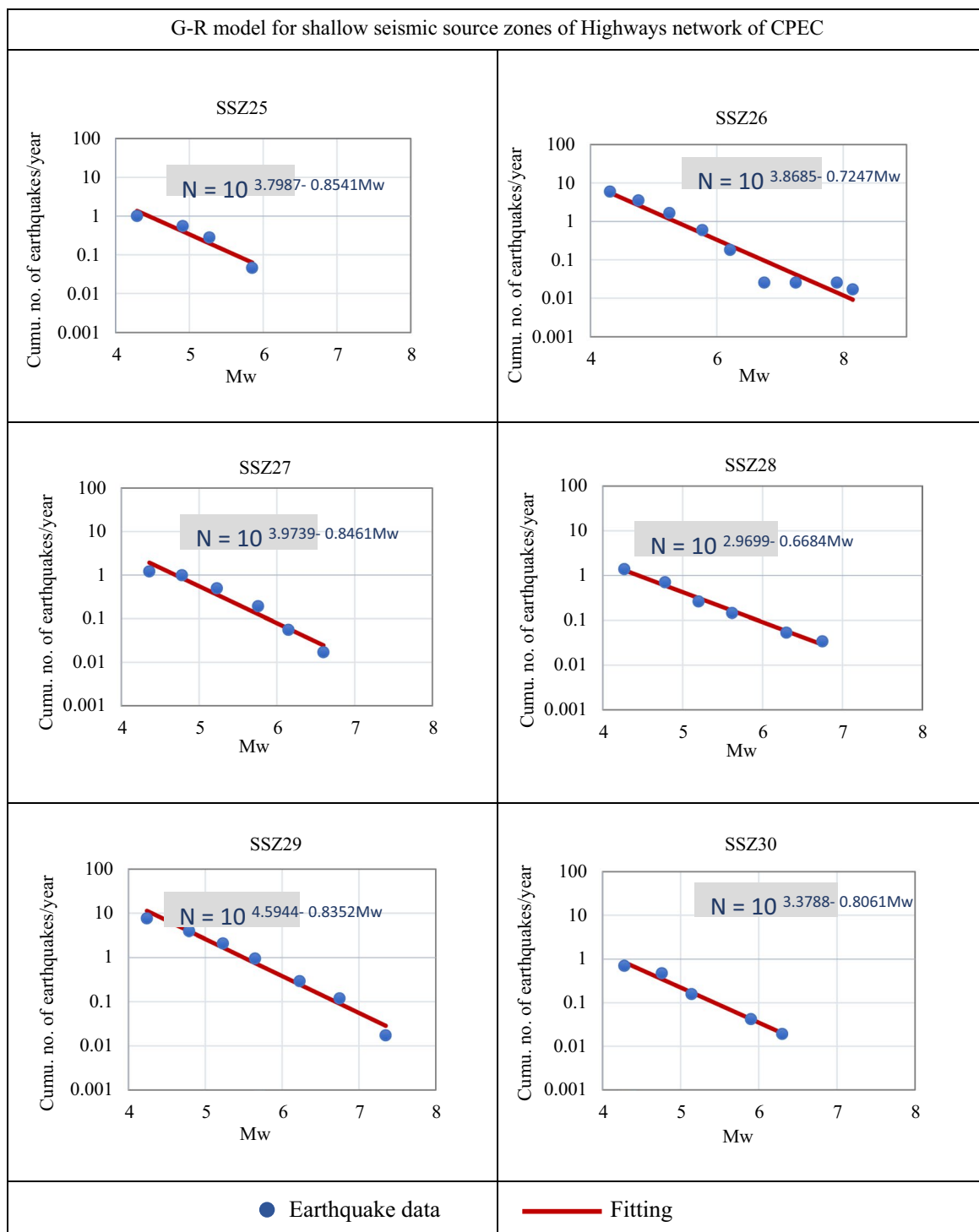**Fig. 7** continued

Fig. 7 continued

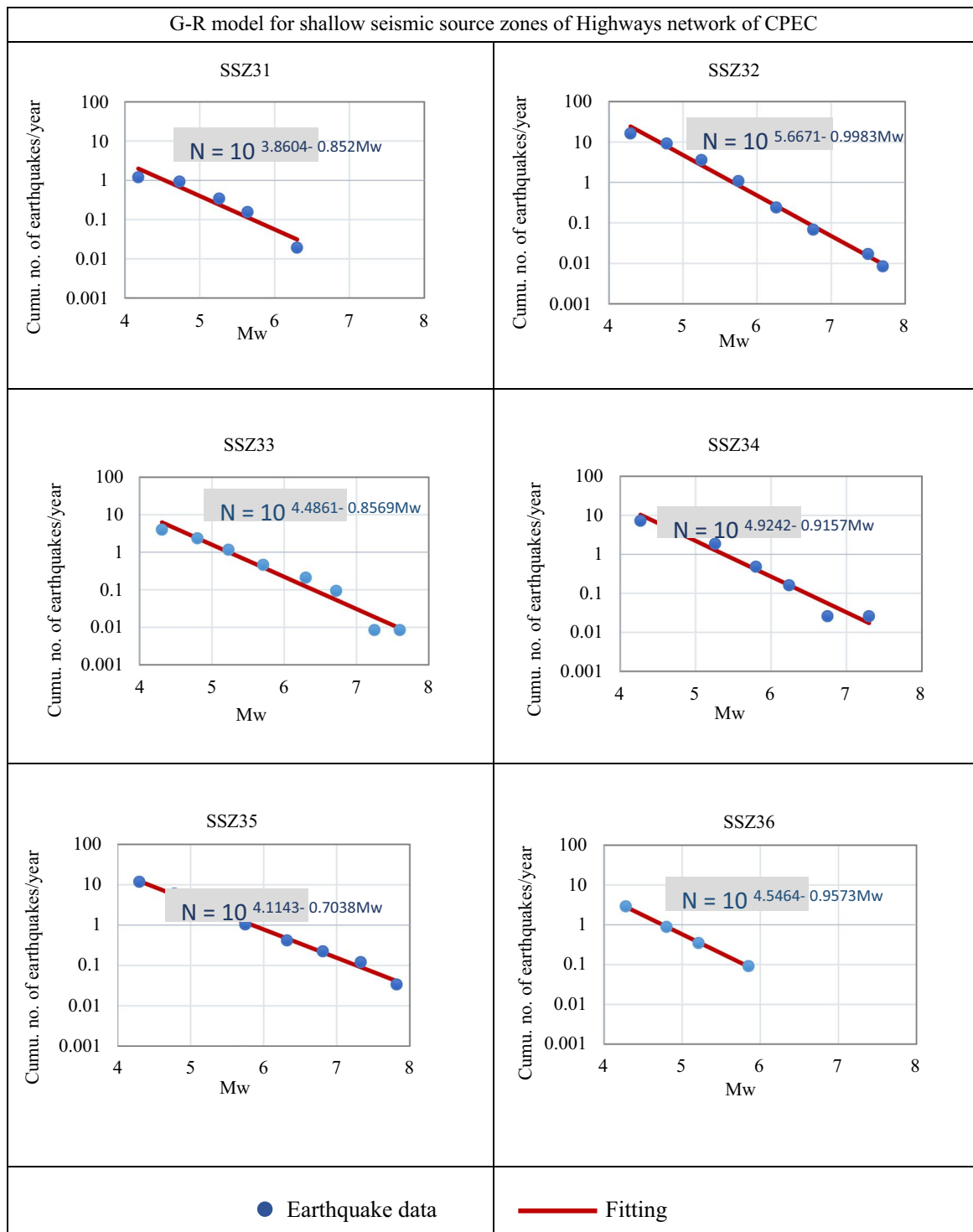**Fig. 7** continued

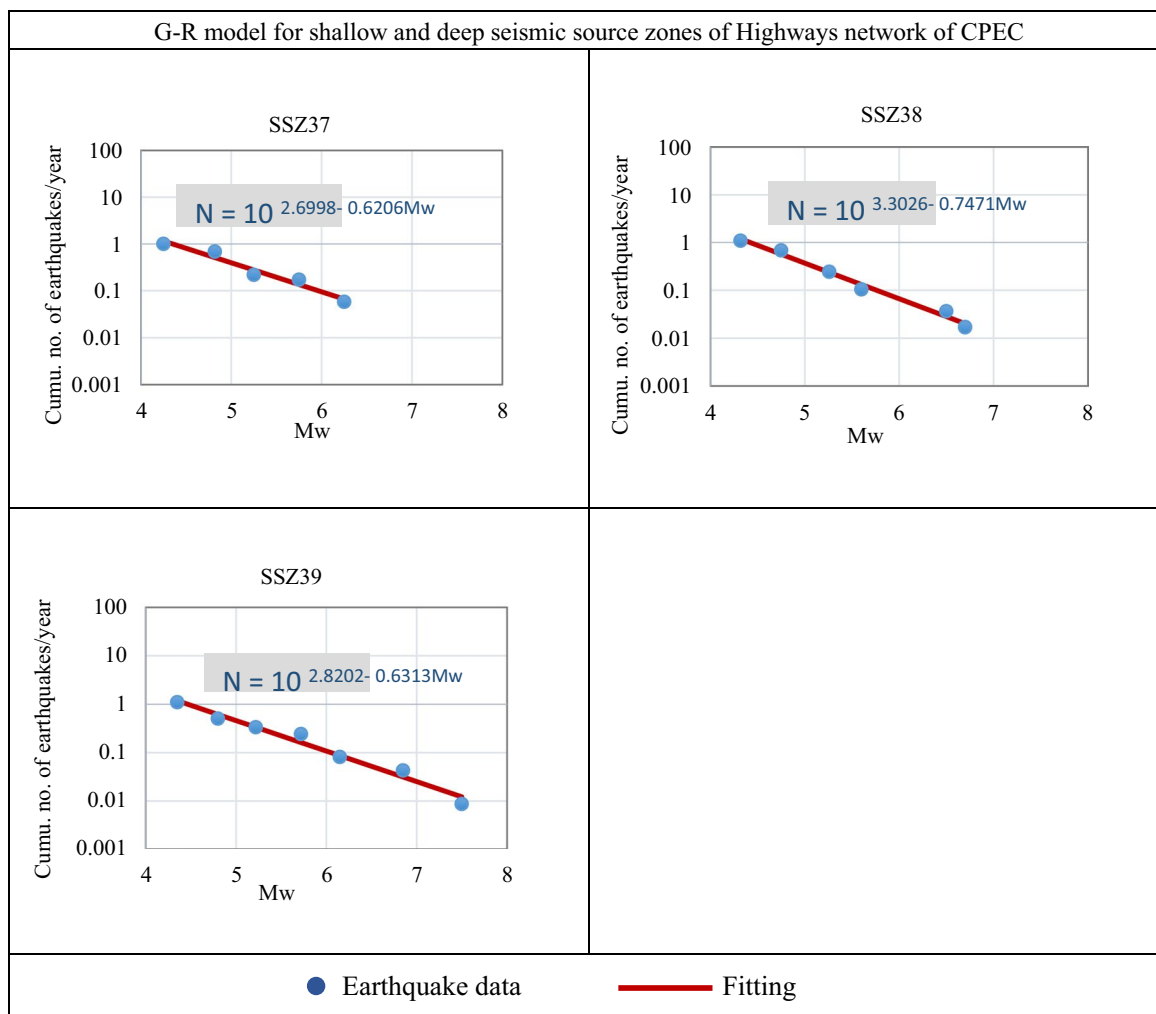**Fig. 7** continued

Fig. 7 continued

Fig. 7 continued

The threshold magnitude, M_w 4.0, was regarded as the minimum engineering magnitude that might cause damage and is thus important in earthquake engineering. Table 2 shows the calculated G–R parameters for each seismic source zone. Figure 7 shows the Gutenberg–Richter model for seismic source zones (1–39) for the CPEC routes.

3.7 Ground motion prediction equations

The reliable ground motion prediction equations for a particular location can be used to generate an accurate estimate of ground motion and spectral acceleration intensity values based on different rates of exceedance. Such an estimate is grounded on strong-motion data in addition to the geology and tectonics of the area. Ground motion prediction equations have not been developed in regions such as Pakistan; therefore, selecting suitable GMPEs based on the region's geology and tectonics is challenging. In Pakistan, there are

three broad tectonic settings: (1) active shallow crustal regions such as the Himalayas, Sulaiman, Kirther, and Chaman regions; (2) the Makran subduction interface zone in the southwestern part of Pakistan; and (3) the subduction intraslab zone in the Pamir, Hindukush, Karakoram, and Himalayas (Waseem et al. 2020). The current study's criterion for selecting globally recognized GMPEs is based on similar tectonic settings. In this study, the ground motion prediction equations developed for similar tectonic regions have been selected randomly from the set of equations. These equations are assigned equal weights in the logic tree and more than one equation is assigned to different tectonic settings of Pakistan. Strong motion data are also scarce due to a lack of different data sharing agencies in Pakistan responsible for earthquake data acquisition. Only PGA values for unknown recording locations are available without the metadata. These PGA values are

established for shallow earthquakes in northern Pakistan. Likewise, the data from the subduction interface zone along the Makran Subduction Zone in Pakistan are also not available. The only study about the evaluation of global ground motion prediction equations is available by Waseem et al. (2022) that was published after the submission of the current study. Therefore, for this study, random selection from the set of well-established ground motion prediction equations from literature is considered. The ground motion data used in the analysis is divided into shallow and deep earthquakes based on a 50-km focal depth dividing line. For the subduction interface/intraslab regions, earthquake events with focal depths greater than 50 km are considered; however, for the active shallow crust regions, earthquake events with focal depths up to 50 km are considered. The four GMPEs are selected at random, and each tectonic zone is assigned two GMPEs. The GMPEs of Boore et al. (2014) and Akkar et al. (2014) are considered for shallow active areas (SSZ 1 to 34, except SSZ 26), whereas Youngs et al. (1997) and Zhao et al. (2006) are considered for the subduction interface/intraslab (SSZ 26, 35–39).

The GMPE of Boore et al. (2014), developed using next-generation attenuation models, predicts the PGA for shallow crustal earthquakes and has a moderate functional form. The required site parameters are Vs30 (average shear wave velocity from surface up to a depth of 30 m), depth (in meters) to 1 km/s shear wave velocity layer and magnitude. The secondary variables are depth to the top of the rupture and hypocentral depth. The function form of Boore et al. (2014) for aleatory variability is presented in Eqs. (8, 9, 10, 11, 12):

$$\sigma = \sqrt{\emptyset^2 + \tau^2} \tag{8}$$

$$\tau = \begin{cases} \tau_1 & M_w \le 4.5 \\ \tau_1 + (\tau_2 + \tau_1)(M_w - 4.5) & 4.5 < M_w < 5.5 \\ \tau_2 & M_w \ge 5.5 \end{cases} \tag{9}$$

$$\emptyset = \begin{cases} \emptyset(M_w, r_{jb}) & V_{s,30} \ge V_2 \\ \emptyset(M_w, r_{jb}) - \Delta\emptyset_V \left[\frac{\ln(V_2/V_{s,30})}{\ln(V_2/V_1)} \right] & V_1 \le V_{s,30} \le V_2 \\ \emptyset(M_w, r_{jb}) - \Delta\emptyset_V & V_{s,30} \le V_1 \end{cases} \tag{10}$$

$$\emptyset(M_W, r_{Jb}) = \begin{cases} \emptyset(M_w) & r_{jb} \le R_1 \\ \emptyset(M_w) + \Delta\emptyset_R \left[\frac{\ln\left(r_{jb}/R_1\right)}{\ln\left(R_2/R_1\right)} \right] & R_1 < r_{jb} \le R_2 \\ \emptyset(M_w) + \Delta\emptyset_R & \end{cases} \tag{11}$$

$$\emptyset(M_w) = \begin{cases} \emptyset_1 & M_w \le 4.5 \\ \emptyset_1 + (\emptyset_2 - \emptyset_1)(M_w - 4.5) & 4.5 < M_w < 5.5 \\ \emptyset_2 & M_w \ge 5.5 \end{cases} \tag{12}$$

where $\emptyset$ is intra-event, τ is inter-event variability, $R_1 = 110$, $R_2 = 270$, $\Delta\emptyset_R = 0.10$, $\Delta\emptyset_V = 0.07$, $V_1 = 225$, $V_2 = 300$, $\emptyset_1 = 0.695$, $\emptyset_2 = 0.495$, $\tau_1 = 0.398$ and $\tau_2 = 0.348$.

The GPME of Akkar et al. (2014) forecasts the pseudo-response continuum for 5% damping up to 4.0 s and is developed for active shallow crust regions. The equations are derived by using a reference data set of ground motions in Europe (RESORCE) and the Middle East region, which is comprised of 1041 records from 221 earthquakes. The required distance parameter is 'Joyner–Boore' distance, the rupture parameter is magnitude, and the site parameter is Vs30. The functional form of Akkar et al. (2014) is presented in Eqs. (13,14,15) (for $M \le 6.75$) is:

$$\ln(Y) = \ln(Y_{REF}) + \ln[S(V_{s,30}, PGA_{REF}) \tag{13}$$

where $\ln(Y_{REF})$ is the reference ground motion model:

$$\ln(Y_{REF}) = \begin{cases} a_1 + a_2(M_w - c_1) + a_3(8.5 - M_w)^2 + [a_4 + a_5(M_w - c_1)]\ln\sqrt{R^2 + a_6^2} + a_8 F_N + a_9 F_R & M_w \le 6.75 \\ a_1 + a_7(M_w - c_1) + a_3(8.5 - M_w)^2 + [a_4 + a_5(M_w - c_1)]\ln\sqrt{R^2 + a_6^2} + a_8 F_N + a_9 F_R & M_w > 6.75 \end{cases} \tag{14}$$

And $\ln[S9(V_{s,30}, PGA_{REF})$ is the nonlinear site amplification function:

$$\ln[S(V_{s,30}, PGA_{REF})] = \begin{cases} b_1 \ln\left(V_{s,30}/V_{REF}\right) + b_2 \ln\left[\frac{PGA_{REF} + C\left(V_{s,30}/V_{REF}\right)^n}{(PGA_{REF} + C)\left(V_{s,30}/V_{REF}\right)^n} \right] & V_{s,30} \le V_{REF} \\ b_1 \ln\left[\frac{\min(V_{s,30}, V_{CON})}{V_{REF}} \right] & V_{s,30} > V_{REF} \end{cases} \tag{15}$$

In these equations, R is the source-site distance measure; Y is the ground motion intensity measure in g; F_N and F_R are the dummy variables used to represent the different fault classes; V_{REF} and V_{CON} are the reference $V_{s,30}$ in the nonlinear site model and the limiting $V_{s,30}$ after which the site amplification is a constant of 750 m/s and 1000 m/s, respectively. The values agreed for other coefficients are, $a_8 = -0.191$, $a_9 = 0.0937$, $a_5 = 0.2529$, $a_6 = 7.5$, $a_7 = -0.5096$, $a_2 = 0.0029$ for all distance metrics. $a_1 = 1.85329$, $a_3 = -0.02807$, $a_4 = -1.23452$, $c_1 = 6.75$, $V_{REF} = 750\ \frac{m}{s}$, $V_{CON} = 1000\ \frac{m}{s}$, $b_1 = -0.41997$, $b_2 = -0.28846$, $c = 2.5$, $n = 3.2$.

The GMPEs of Youngs et al. (1997) and Zhao et al. (2006) were developed for subduction intraslab and interface regions such as Japan, Cascadia, and Alaska. The required site parameter for GMPE Youngs et al. (1997) is Vs30, rupture parameters are magnitude and focal depth. The function of Youngs et al. (1997) is presented in Eq. (16) is:

$$\ln \text{PGA} = C_1^* + C_2 M + C_3^* \ln \left[r_{\text{rup}} + e^{C_4^* - \frac{C_2}{C_3^*} M} \right] + C_5 Z_{ss} + C_8 Z_t + C_9 H \tag{16}$$

whereas $C_1^* = C_1 + C_3 C_4 - C_3^* C_4^*, C_3^* = C_3 + C_6 Z_{ss}, C_4^* = C_4 + C_7 Z_{ss}$.

In this equation, PGA is measured in g, $C_1 = 0.2418$, $C_2 = 1.414$, $C_3 = -2.552$, $C_4 = \ln(1.7818)$, $C_8 = 0.3846$, $C_9 = 0.00607$, and $\sigma = 1.45 - 0.1M$. The other coefficients are not needed for prediction in rock. The tectonic type of the equation is interface and intraslab with a focal depth, H, between 10 and 229 km. In this equation, the effect of depth and tectonic type is significant.

The GMPE of Zhao et al. (2006) implements the equations for the subduction interface. The required rupture parameters are the magnitude and focal depth.

The function form of Zhao et al. (2006) is presented in Eq. (17):

$$\log_e (y) = aM_w + bx - \log_e (r) + e(h - h_c)\delta_h + F_R + S_I + S_S + S_{SL} \log_e (x) + C_k \tag{17}$$

where

$$r = x + C \exp (dM_w)$$

where y is in cm/s², $\delta_h = 1$ when $h \geq h_c$ and 0 otherwise, $a = 1.101$, $b = -0.00564$, $c = 0.0055$, $d = 1.080$, $e = 0.014112$, $S_I = 0.000$, $S_S = 2.607$, $S_{SL} = -0.528$, $C_H = 0.293$, $C_1 = 1.111$, $C_2 = 1.344$, $C_3 = 1.355$, $C_4 = 1.420$, $h = $ focal depth, $h_c = 15$ km (best depth effect for shallow events), $\sigma = 0.604$ (intra-event) and $\tau = 0.398$ (inter-event). The equation classifies events into three source types; (1) Crustal, (2) Interface S_I, (3) Slab S_S and S_{SL}. F_R is about faulting mechanisms. Hard rock NEHRP site class A, $V_{s,30} > 1100$ m/s, C_H is used. The equation provides a reasonable distribution with respect to magnitude and depth.

All the GMPEs employed are well recognized and are used to compute seismic hazard analysis. Figure 8 shows the logic tree approach used in the study.

3.8 Epistemic uncertainties

The epistemic uncertainty in the computation of seismic hazard analysis is concerned with the lack of knowledge about earthquakes and ground motions. These uncertainties are well expressed using a logic tree, and the weight assigned to the respective logic tree branch illustrates the confidence level of the analyst. The logic tree branches are mainly associated with the approach adopted for the hazard analysis, source model, the selection of GMPEs, and source characterization. Figure 8 shows the logic
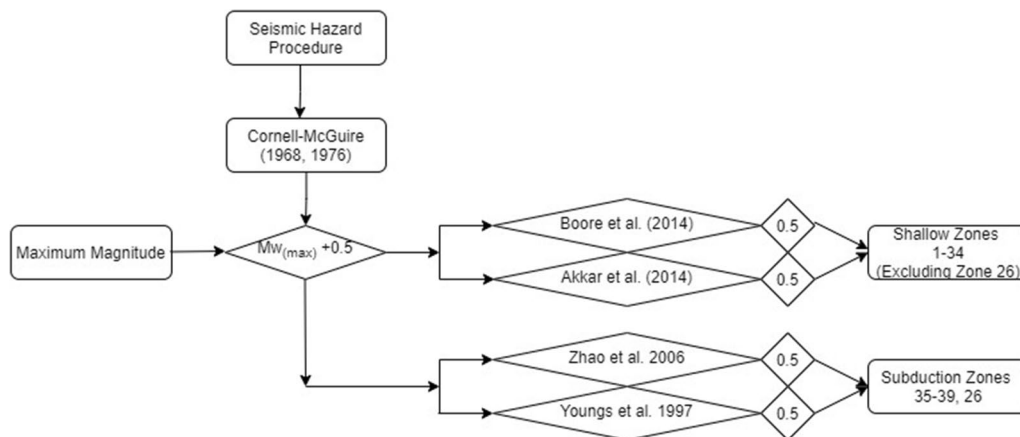

Fig. 8 The logic tree approach, which assigns equal weights to each GMPE. This approach implies that each equation has an equal likelihood of providing accurate predictions of ground motion
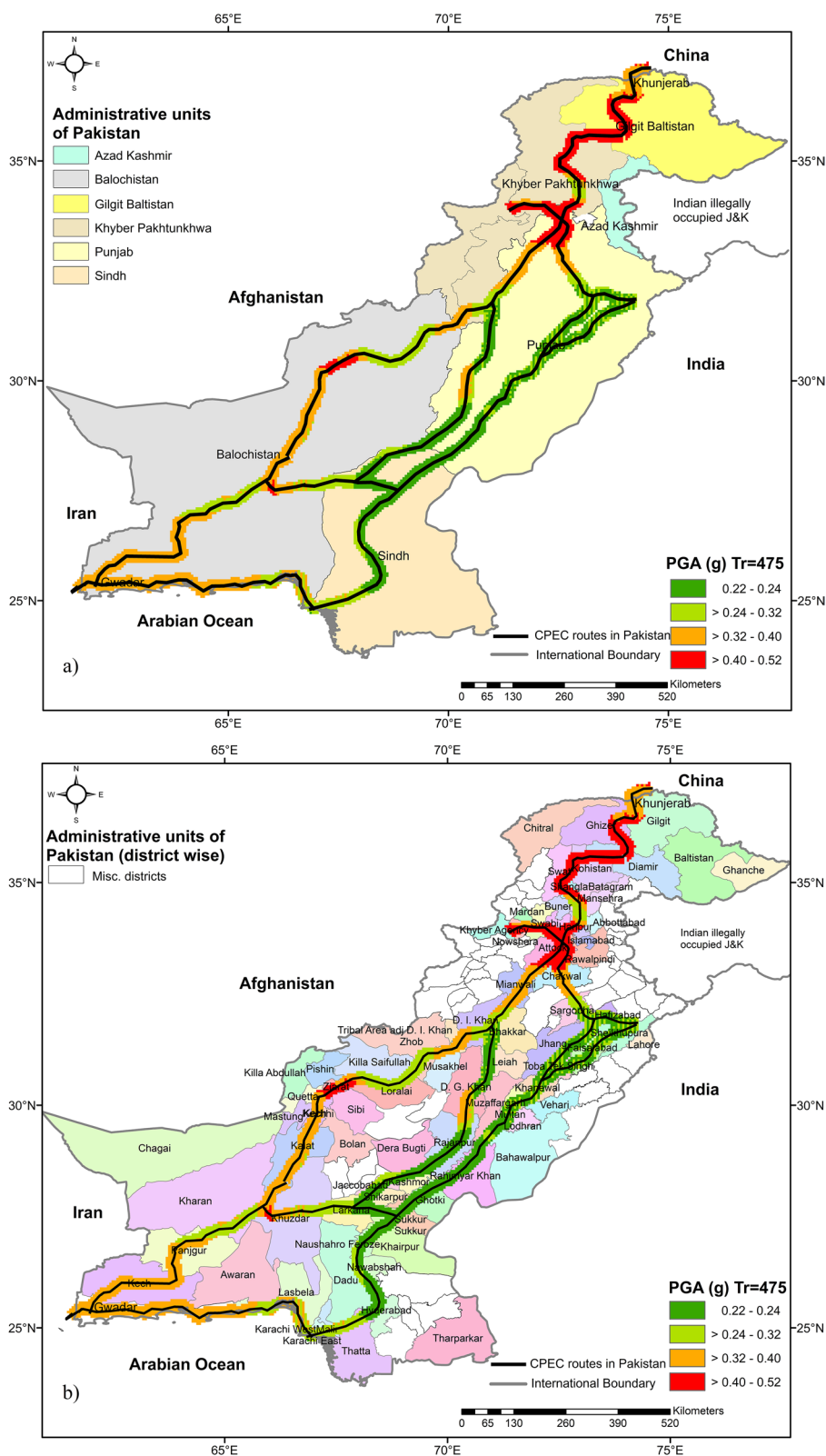
Fig. 9 Seismic hazard maps of CPEC routes in terms of PGA for 475-year return period. **a** The province-wise maps show the SA values for each province along the CPEC routes, **b** the district-wise maps provide a more granular view of the seismic hazard by showing the SA values for individual districts
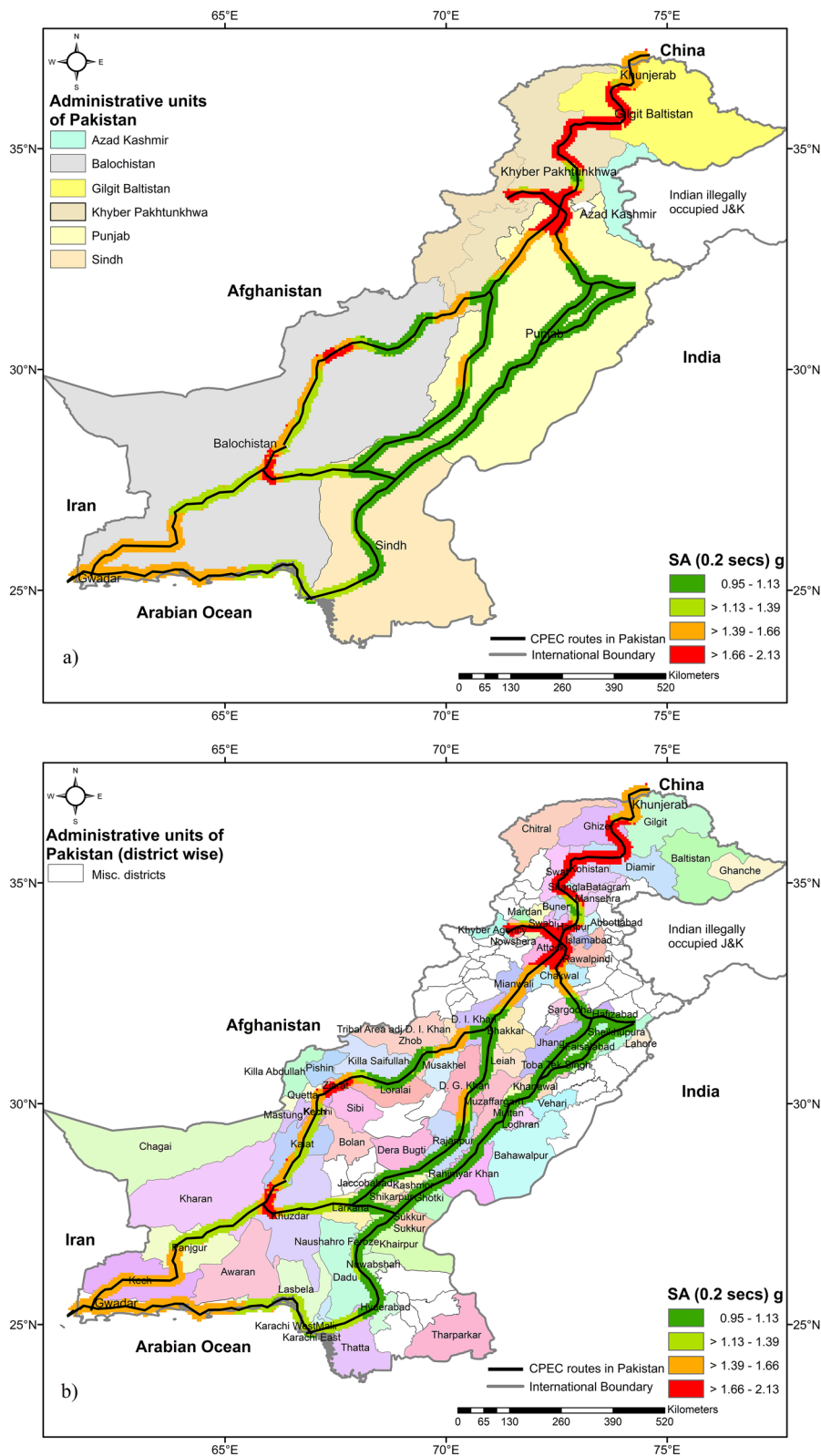
Fig. 10 Seismic hazard maps of CPEC routes in terms of PGA for 2475-year return period. **a** The province-wise maps show the SA values for each province along the CPEC routes **b** the district-wise maps provide a more granular view of the seismic hazard by showing the SA values for individual districts

Fig. 11 Seismic hazard maps of CPEC routes in terms of SA at *T* = 0.2 s for 2475-year return period. **a** The province-wise maps show the SA values for each province along the CPEC routes **b** the district-wise maps provide a more granular view of the seismic hazard by showing the SA values for individual districts

tree approach used in the study. The logic tree approach is only developed for attenuation equations in the current study. Each attenuation equation is assigned equal weight (0.5) to preserve equal uncertainty in the assessment.

4   Results and discussion

The province- and district-wise seismic hazard maps for the CPEC routes in terms of PGA for 475- and 2475-year RPs are shown in Figs. 9 and 10. For engineering bedrock site conditions, these maps are in agreement (i.e., Vs30 of 760 m/s). The color-coded maps signify the amplitude deviation of ground motion parameters. According to the overall spatial evaluation of seismic hazard maps, the northern and western CPEC routes are prone to the highest seismic hazard levels, i.e., the attained PGA values are in the range of 0.40–0.52 g for 475-year RP. This is due to the proximity of multiple active faults in the Hindukush, Himalayan, Karakoram, and Sulaiman mountains, whereas the central and eastern CPEC routes have comparatively lower seismic hazard levels for 475-year RP (Fig. 9a). The western CPEC route, which passes through the districts of Ziarat, Quetta, Sibi and is next to the Sulaiman fold belt and the Bella Chaman Kurram fault zone, is likewise seismically hazardous, with PGA values ranging from 0.40 to 0.52 g for 475-year RP. Intermediate and shallow focus earthquakes are frequent in this region due to the presence of faults such as Kingri, Waziristan-Loralai, Muslim Bagh, Chaman, and Ghaziabad. The northern CPEC route passes through Ghizer, Diamer, Kohistan, Swat, Shangla, Mansehra, Haripur, Islamabad, Attock, Swabi, and Peshawar districts, which is adjacent to the Pamir–Karakoram Mountains, Hindukush–Himalaya ranges, Kohistan Island arc, and suture zones. This route is characterized by high seismicity, with PGA values up to 0.52 g for 475-year RP (Fig. 9b). The region is tectonically active due to the Indian–Eurasian plate collision and has numerous regional faults such as Karakoram, North Pamir, South Pamir, Tirch Mir, Reshun, MMT, MCT, MBT, sinistral Jhelum, Nathiagali, Panjal thrust, Khairabad, and Himalayan frontal thrust. The CPEC route passing through the Mianwali, Zhob, Kachhi, Kalat, Khuzdar, Panjgur, Kech, and Gwadar districts bordering the Chagai arc and Makran subduction zone is recognized as the second most hazardous route, with PGA values ranging between 0.32–0.40 g for 475-year RP (Fig. 9b). The well-known Dalbandin and Ras-Koh faults, as well as a significant number of unidentified faults, are located in the Chagai and Mashkhel areas. The 2011 Dalbandin earthquake (M_w 7.2) and the 1983 Iran earthquake (M_w 7.0) indicated moderate seismicity in the area. In central Makran region, Panjgur and Hoshab faults have generated several intermediate subduction megathrusts. The Makran coastal trough zone is characterized by shallow subduction megathrusts such as the Ormara fault, Makran coast fault, and Makran subduction thrusts (Fig. 1). The zone has high seismicity, as evidenced by the 1945 Makran earthquake (Mw 8.2) and the 2013 Awaran earthquake (M_w 7.7). The central CPEC route is characterized by lower hazard values, i.e., PGA values of 0.22–0.24 g, except in a section of the D.G. Khan district where the ground intensity is approaching 0.40 g for 475-year RP (Fig. 9b). The eastern CPEC route passing through the Indian shield region has been recognized as the less hazardous route for 475-year RP, which may be due to scattered seismicity and a limited number of faults in the region. Figure 10 presents the province- and district-wise color-coded maps for the 2475-year RP with PGA values ranging between 0.43 and 0.93 g.

The spectral acceleration values (SA) computed at $T = 0.2$ s (short-period) and $T = 1.0$ s (long-period) for a 2% risk of exceedance in 50 years (2475-year RP) provided the hazard definition in line with the AASHTO (2012) (Specifications 2012) and IBC (2021) (Ching and Winkel 2021) criteria. Figures 11 and 12 present the province- and district-wise color-coded SA maps at $T = 0.2$ s and 1.0 s for 2475-year RP. These maps are in agreement with engineering bedrock site conditions (i.e., Vs30 of 760 m/s). The spectral acceleration maps reveal that the hazard is not uniformly spread over CPEC routes in Pakistan, with increased hazards observed in the northern and western CPEC routes (Fig. 11a). The presence of faults such as Tirch Mir, Reshun, MBT, Kalabagh, Khairabad, east–west oriented MMT, and MKT in the region results in the highest ground intensity values encountered in the northern CPEC route (Fig. 11b). The maximum ground intensities encountered in the western CPEC route passing through Ziarat, Quetta, Sibi, Kechhi, and Khuzdar districts are owing to the presence of active Chaman, Ghaziabad, and Chaman faults (Fig. 2). For the 2475-year RP, the SA values (0.2 s) and SA (1.0 s) range between 0.95–2.13 g and 0.24–0.64 g, respectively (Figs. 11, 12).

The current study has utilized an updated earthquake catalogue (25AD-2020), reorganized completeness periods, introduced four updated GMPEs, computed activity rates in each source zone, incorporated the 84th percentile of focal depths in each source zone, established a 15-km fishnet grid on either side of the CPEC routes and also used the latest OpenQuake version 3.10 software engine for hazard computation, which makes it exclusive to other studies carried out for the territory of Pakistan, e.g., Building Code of Pakistan (2007), Zaman et al. (2012), and Waseem et al. (2020). Ground motion values are calculated by taking into account both shallow and deep-focus earthquakes. Instead of considering the average focal depth (50%) value within each source zone, the
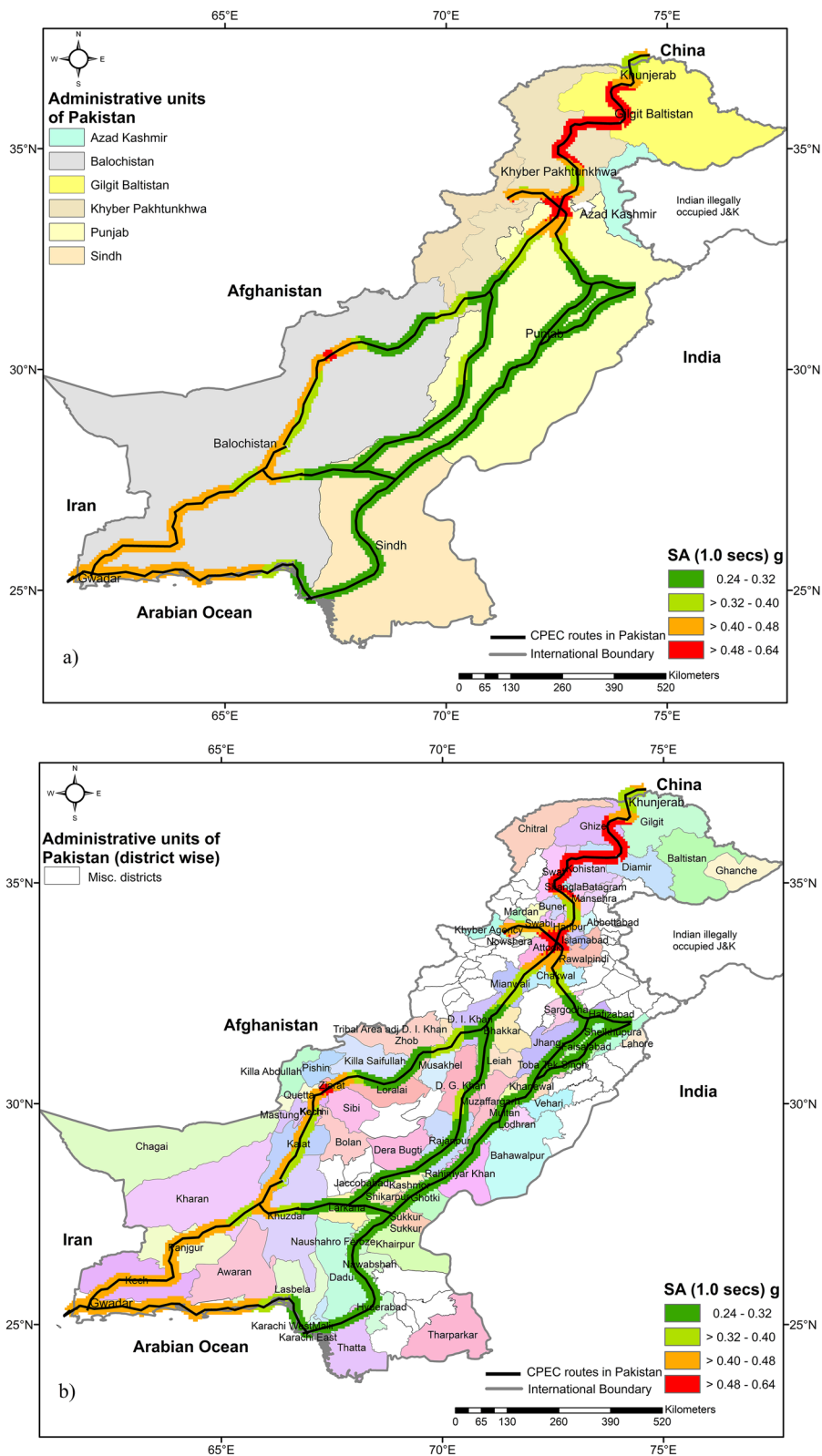
Fig. 12 Seismic hazard maps of CPEC routes in terms of SA at *T* = 1.0 s for 2475-year return period. **a** The province-wise maps show the SA values for each province along the CPEC routes, while **b** the district-wise maps provide a more granular view of the seismic hazard by showing the SA values for individual districts

hypo depth of earthquakes within a source zone is determined by using the 84th percentile of the focal depths (the 50% + one standard deviation of focal depths). Taking the average focal depth (50%) value in a source zone has the effect of abnormally increasing the hazard level within each source zone.

The CPEC routes connect Khunjerab in North Pakistan to Gwadar in South Pakistan and extend throughout the country via their western, central, and eastern routes (Fig. 2). Therefore, a comparison of earlier studies for the territory of Pakistan can be furnished to the CPEC routes in Pakistan based on obtained PGA values. The PGA agreeing to a 10% probability of exceedance in 50 years (475-year RP) is a standard parameter for hazard computation, and hence, a comparison can be established based on this parameter. The maximum PGA value obtained in this study is 0.52 g for the period of 475-year RP, which is consistent with the values obtained by Sesetyan et al. (2018a) and higher than the values obtained by Waseem et al. (2020). They used shear wave velocity of 760 m/s as a site condition, EZ-FRISK software version 7.62, and three sigma of ground motion prediction equations to capture the variation in ground motions. Sesetyan et al. (2018a) have used a shear wave velocity of 750 m/s as a site condition and three standard deviations of ground motion prediction equations. The current study has used 760 m/s shear wave velocity and three standard deviations of equations that are comparable with Waseem et al. (2020) and Sesetyan et al. (2018a) in terms of these parameters. The BCP (2007) study used 760 m/s shear wave velocity and one standard deviation of ground motion prediction equation. Complete information is not available for all the mentioned studies; therefore, it may be safely assumed that they have followed the variation in ground motion and rock site conditions to evaluate the ground motion hazard. This study is also comparable to the studies of the BCP (2007), and the Global Seismic Hazard Assessment Programme (GSHAP) by Zhang et al. (1999) due to similarity in the hazard computation approach and source models. However, BCP has classified Pakistan into five seismic zones, with the highest attainable PGA value marked as greater than 0.32 g and no upper bound value is provided for the 475-year RP. The equivalent PGA values obtained in this study vary from 0.22–0.52 g for the CPEC routes in Pakistan, utilizing an aerial source for 475 year RP (Fig. 9). The spatial distribution of these PGA values obtained for the CPEC routes in Pakistan can be equally helpful in Pakistan's revised seismic zonation map. According to Zhang et al. (1999), Rafi et al. (2012), Sesetyan et al. (2018a), and Waseem et al. (2020), the attained PGA values range between 0.04–0.50 g, 0.004–0.22 g, 0.02–0.50 g, and 0.15–0.40 g, for 475-year RP, respectively. The results of

Zhang et al. (1999) and Sesetyan et al. (2018a) agree with the upper bound of attained PGA values in the current study. However, the results of Waseem et al. (2020) are slightly lower than the upper bound but in agreement with the lower bound of attained PGA values for the territory of Pakistan.

The ground motion intensity values obtained in this study (i.e., PGA and SA) may be used for all types of infrastructure, particularly the spectral intensity values for the seismic design of the bridges along with the CPEC routes under AASHTO (2012) and IBC (2021) guidelines. The PGA and SA maps can be a way forward to adopt structural mitigation measures for all kinds of infrastructure being built around and across the CPEC routes in Pakistan to make these routes secure and productive.

5 Conclusions

The result of the probabilistic seismic hazard assessment offers rationalized seismic hazard maps for the CPEC routes in Pakistan. This research leads to the following conclusions:

1. The highest seismic hazard is apparent in the northern and western CPEC routes in Pakistan due to active tectonic features in the vicinity of these sections. The industrial zones, transport infrastructure, and tunnels built along these routes are vulnerable, even to small ground motion intensities.
2. The western CPEC route in Pakistan, which passes through Ziarat, Quetta, and Sibi districts adjacent to the Sulaiman fold belt and the Bella Chaman Kurram fault zone, is the most seismically hazardous route, with attained PGA values ranging between 0.40 and 0.52 g for 475-year RP and SA (0.2 s) values ranging between 1.66 and 2.13 g for 2475-year RP. The routes with highest PGA values are more prone to seismic risk and vulnerability. This highway section contains many active faults in the neighborhood (i.e., the Chaman fault, Ghaziabad fault, Muslim Bagh fault, and Waziristan-Loralai fault). The planned CPEC infrastructure projects like hospitals, educational institutes, and roads build along this route are more vulnerable to seismic hazard.
3. The continuation of the western CPEC runs adjacent to the Makran subduction zone and Chagai arc, considerably passing through Zhob, Kachhi, Kalat, Khuzdar, Panjgur, Kech, and Gwadar districts are characterized as the second most hazardous route, i.e., PGA value ranges between 0.32 and 0.40 g for 475-year RP and SA (0.2 s) values ranges between 1.39 and 1.66 g for 2475-year RP. The planned CPEC projects like the Gwadar airport and energy plants

Rehman *et al. Progress in Earth and Planetary Science*   (2023) 10:27

Page 29 of 31

(coal, wind, solar) can be designed by following the attained accelerations values for earthquake-resistant structures.

4. The central and eastern CPEC routes are generally characterized by lower hazard values, i.e., PGA values range between 0.22–0.24 g for 475-year RP and SA (0.2 s) values range between 0.95 and 1.13 g for 2475-year RP, except in a highway section of D.G. Khan district where the ground acceleration approaches 0.40 g for 475-year RP may be due to the presence of Sulaiman fold and thrust belt (Zindapir anticlinal zone).

5. The peak ground acceleration (PGA) values achieved at 10% and 2% probability of exceedance in 50 years and spectral acceleration values (SA) obtained at $T=0.2$ s and $T=1.0$ s for 2% probability of exceedance in 50 years provides hazard definition in accordance with the AASHTO LRFD (2012) and IBC (2021) recommendations and can be used for seismic design of any type of infrastructure built along the CPEC routes.

Author contributions
Conceptualization, Q.R., M.W., W.A.; methodology, Q.R., M.W., W.A.; software, Q.R.; validation, Q.R., M.W., W.A., I.I, H.T.J., G.K.; formal analysis, Q.R.; investigation, Q.R., M.W., W.A., I.I, H.T.J., G.K.; resources, M.W., W.A.; data curation, Q.R., M.W., W.A.; writing—original draft preparation, W.A.; writing—review and editing, Q.R., M.W., W.A.; I.I, H.T.J., G.K.; visualization, Q.R., M.W., W.A, I.I, H.T.J G.K.; supervision, M.W., W.A. All authors read and approved the final manuscript.

Availability of data and materials
The data used in this work is available on request.

Declarations

Ethics approval and consent to participate
Not applicable.

Consent for publication
Not applicable.

Competing interests
The author declares no competing interests.

Author details
[1]National Centre of Excellence in Geology, University of Peshawar, Peshawar 25120, Pakistan. [2]Department of Earth Sciences, University of Haripur, Haripur 22610, Pakistan. [3]Department of Civil Engineering, University of Engineering and Technology, Peshawar 25120, Pakistan. [4]Department of Geology, Shaheed Benazir Bhutto University Sheringal, Upper Dir 18000, Khyber Pakhtunkhwa, Pakistan. [5]Department of Historical Geology-Paleontology, Faculty of Geology and Geoenvironment, School of Earth Sciences, National and Kapodistrian University of Athens, Panepistimiopolis, Zografou, 15784 Athens, Greece.

References
AASHTO-LRFD (2012) Bridge design specifications, 6th ed. American Association of State Highway and Transportation Officials, Washington, DC. ISBN: 978-1-56051-523-4

Akkar S, Sandıkkaya MA, Bommer JJ (2014) Empirical ground-motion models for point-and extended-source crustal earthquake scenarios in Europe and the Middle East. Bull Earthq Eng 12(1):359–387. https://doi.org/10.1007/s10518-013-9461-4

Basharat M, Rohn J, Ehret D, Baig MS (2012) Lithological and structural control of Hattian Bala rock avalanche triggered by the Kashmir earthquake 2005, sub-Himalayas, northern Pakistan. J Earth Sci 23(2):213–224. https://doi.org/10.1007/s12583-012-0248-3

BCP. Building Code of Pakistan with Seismic Provisions (2007) Minist. Hous. Work. Government of Pakistan Islamabad

Bignold SM, Treloar PJ (2003) Northward subduction of the Indian Plate beneath the Kohistan island arc, Pakistan Himalaya: new evidence from isotopic data. J Geol Soc Lond 160(3):377–84. https://doi.org/10.1144/0016-764902-068

Bilham R (1999) Slip parameters for the Rann of Kachchh, India, 16 June 1819, earthquake, quantified from contemporary accounts. Geol Soc Lond Spec Publ 146(1):295–319. https://doi.org/10.1144/GSL.SP.1999.146.01.18

Bilham R, Lodi S, Hough S, Bukhary S, Khan AM, Rafeeqi SFA (2007) Seismic hazard in Karachi, Pakistan: uncertain past, uncertain future. Seismol Res Lett Seismol Soc Am 78(6):601–613. https://doi.org/10.1785/gssrl.78.6.601

Boore DM, Stewart JP, Seyhan E, Atkinson GM (2014) NGA-West2 equations for predicting PGA, PGV, and 5% damped PSA for shallow crustal earthquakes. Earthq Spectra Earthq Eng Res Inst 30(3):1057–1085. https://doi.org/10.1193/070113EQS184M

Chang M, Cui P, Dou X, Su F (2021) Quantitative risk assessment of landslides over the China–Pakistan economic corridor. Int J Disaster Risk Reduct 63:102441. https://doi.org/10.1016/j.ijdrr.2021.102441

Chaudhry MN, Ghazanfar M (1990) Position of the Main Central Thrust in the tectonic framework of Western Himalaya. Tectonophysics 174(3–4):321–329. https://doi.org/10.1016/0040-1951(90)90329-7

Ching FDK, Winkel SR (2021) Building codes illustrated: a guide to understanding the 2021 international building code. Wiley. ISBN: 978-1-119-77240-8

Cook N, Butz D (2015) The dialectical constitution of mobility and immobility: recovering from the Attabad Landslide disaster, Gojal, Gilgit-Baltistan, Pakistan. Contemp South Asia 23(4):388–408. https://doi.org/10.1080/09584935.2015.1090950

Ding L, Qasim M, Jadoon IAK, Khan MA, Xu Q, Cai F, Wang H, Baral U, Yue Y (2016) The India–Asia collision in north Pakistan: insight from the U–Pb detrital zircon provenance of Cenozoic foreland basin. Earth Planet Sci Lett 455:49–61. https://doi.org/10.1016/j.epsl.2016.09.003

Fan F, Xiao C, Feng Z, Chen Y (2022) Land-planning management based on multiple ecosystem services and simulation in tropical forests. J Environ Manag 323:116216. https://doi.org/10.1016/j.jenvmen.2022.116216

Farah A, DeJong KA (1984) Geodynamics of Pakistan. Geological Survey of Pakistan

Farah A, Lawrence RD, DeJong KA (1979) An overview of the tectonics of Pakistan. Mar Geol Oceanogr Arab Sea Coast Pak. Van Nostrand Reinhold Company, New York, pp 161–176

Fattahi H, Amelung F (2016) InSAR observations of strain accumulation and fault creep along the Chaman Fault system, Pakistan and Afghanistan. Geophys Res Lett 43(16):8399–8406. https://doi.org/10.1002/2016GL070121

Fujiwara S, Tobita M, Sato HP, Ozawa S, Une H, Koarai M, Nakai H, Fujiwara M, Yarai H, Nishimura T, Hayashi F (2006) Satellite data gives snapshot of the

2005 Pakistan earthquake. Eos Trans Am Geophys Union 87(7):73–77. https://doi.org/10.1029/2006EO070001

Gardner JK, Knopoff L (1974) Is the sequence of earthquakes in Southern California, with aftershocks removed, Poissonian? Bull Seismol Soc Am Citeseer 64(5):1363–1367

Gutenberg B, Richter CF (1956) Earthquake magnitude, intensity, energy, and acceleration: (second paper). Bull Seismol Soc Am 46(2):105–145. https://doi.org/10.1785/BSSA0460020105

Irshad MS (2015) One belt and one road: Dose China–Pakistan economic corridor benefit for Pakistan's economy? J Econ Sustain Dev 6(24):66

Jadoon IAK, Khurshid A (1996) Gravity and tectonic model across the Sulaiman fold belt and the Chaman fault zone in western Pakistan and eastern Afghanistan. Tectonophysics 254(1–2):89–109. https://doi.org/10.1016/0040-1951(95)00078-X

Jadoon IAK, Lawrence RD, Lillie RJ (1992) Balanced and retrodeformed geological cross-section from the frontal Sulaiman Lobe, Pakistan: duplex development in thick strata along the western margin of the Indian Plate. Thrust Tectonics 66:343–356

Jadoon IAK, Lawrence RD, Lillie RJ (1994) Seismic data, geometry, evolution, and shortening in the active Sulaiman fold-and-thrust belt of Pakistan, southwest of the Himalayas. Am Assoc Pet Geol Bull 8(5):758–774

Jagoutz O, Schmidt MW (2012) The formation and bulk composition of modern juvenile continental crust: the Kohistan arc. Chem Geol 298:79–96. https://doi.org/10.1016/j.chemgeo.2011.10.022

Karim D, Karim I, Daveel S, Khan A (2015) Damming hunza river by massive Attabad landslide, story of a risk management initiative from Hunza, Pakistan. J Mt Area Res 5:1–9. https://doi.org/10.53874/jmar.v5i0.76

Khan S, Waseem M, Khan MA, Ahmed W (2018) Updated earthquake catalogue for seismic hazard analysis in Pakistan. J Seismol 22(4):841–861. https://doi.org/10.1007/s10950-018-9736-y

Kramer SL (1996) Geotechnical earthquake engineering. Pearson Education, India

Lawrence RD, Yeats RS, Khan SH, Farah A, DeJong KA (1981) Thrust and strike slip fault interaction along the Chaman transform zone, Pakistan. Geol Soc Lond Spec Publ 9(1):363–70. https://doi.org/10.1144/GSL.SP.1981.009.01

Mahmood K, Ahmad N, Khan U, Iqbal Q (2020) Seismic hazard maps of Peshawar District for various return periods. Nat Hazards Earth Syst Sci 20:1639–1661. https://doi.org/10.5194/nhess-20-1639-2020

Makhdoom AS, Shah AB, Sami K (2018) Pakistan on the roadway to socio-economic development: a comprehensive study of China Pakistan Economic Corridor (CPEC). Gov Res J Polit Sci 6(6):66

Malkani MS, Mahmood Z (2016) Fluorite from Loralai-Mekhtar and Celestite from Barkhan, Dera Bugti, Kohlu, Loralai and Musakhel districts (Sulaiman Foldbelt) and Karkh area of Khuzdar district (Kirthar Range): a glimpse on Tectonic and Sedimentary Mineral Resources of Indus Basin Pak. Geol. Surv. Pakistan. Inf Release 980:1–16

Monalisa KAA, Jan MQ (2007) Seismic hazard assessment of the NW Himalayan fold-and-thrust belt, Pakistan, using probabilistic approach. J Earthq Eng 11(2):257–301. https://doi.org/10.1080/13632460601031243

Mukhopadhyay B, Dasgupta S (2015) Seismic hazard assessment of Kashmir and Kangra valley region, Western Himalaya, India. Geomat Nat Hazards Risk 6(2):149–183. https://doi.org/10.1080/19475705.2013.832405

Naseer A, Khan AN, Hussain Z, Ali Q (2010) Observed seismic behavior of buildings in northern Pakistan during the 2005 Kashmir earthquake. Earthq Spectra Earthq Eng Res Inst 26(2):425–449. https://doi.org/10.1193/1.3383119

Pagani M, Silva V, Rao A, Simionato M, Johnson K (2023) OpenQuake engine manual

Petterson MG (2010) A review of the geology and tectonics of the Kohistan island arc, north Pakistan. Geol Soc London Spec Publ 338(1):287–327.https://doi.org/10.1144/SP338.14

Petterson MG, Windley BF (1985) RbSr dating of the Kohistan arc-batholith in the Trans-Himalaya of north Pakistan, and tectonic implications. Earth Planet Sci Lett 74(1):45–57. https://doi.org/10.1016/0012-821X(85)90165-7

Qasim M, Ding L, Khan MA, Jadoon IA, Haneef M, Baral U, Cai F, Wang H, Yue Y (2018) Tectonic implications of detrital zircon ages from lesser Himalayan Mesozoic-Cenozoic strata, Pakistan. Geochem Geophys Geosyst 19(5):1636–1659. https://doi.org/10.1002/2017GC006895

Rafi Z, Lindholm C, Bungum H, Laghari A, Ahmed N (2012) Probabilistic seismic hazard of Pakistan, Azad-Jammu and Kashmir. Nat Hazards 61(3):1317–1354. https://doi.org/10.1007/s11069-011-9984-4

Rahman MM, Bai L, Khan NG, Li G (2019) Probabilistic seismic hazard assessment for Himalayan–tibetan region from historical and instrumental earthquake catalogs. Earthqu Multi-Hazards Around Pac Rim 2:161–181. https://doi.org/10.1007/s00024-017-1659-y

Rehman G, Ahmad S, Khan SD, Ali F, Ali TH, Khan SF (2014) Threat of glacial lake outburst flood to Tehsil Gupis from Khukush Lake, District Ghizer, Gilgit Baltistan, Pakistan. Nat Hazards 70(2):1589–1602. https://doi.org/10.1007/s11069-013-0893-6

Rehman HU, Seno T, Yamamoto H, Khan T (2011) Timing of collision of the Kohistan–Ladakh Arc with India and Asia: debate. Isl Arc 20(3):308–328. https://doi.org/10.1111/j.1440-1738.2011.00774.x

Rehman QU, Ahmed W, Waseem M, Khan S, Farid A, Shah SHA (2021) Geophysical investigations of a potential landslide area in Mayoon, Hunza District, Gilgit-Baltistan, Pakistan. Rud Zb Bull 36(3):66

Searle MP, Khan MA, Fraser JE, Gough SJ, Jan MQ (1999) The tectonic evolution of the Kohistan-Karakoram collision belt along the Karakoram Highway transect, north Pakistan. Tectonics 18(6):929–949. https://doi.org/10.1029/1999TC900042

Sesetyan K, Danciu L, Demircioglu MB, Giardini D, Erdik M, Akkar S, Gülen L, Zare M, Adamia S, Ansari A, Arakelyan A (2018a) The 2014 seismic hazard model of the Middle East: overview and results. Bull Earthq Eng 16:3535–3566. https://doi.org/10.1007/s10518-018-0346-4

Sesetyan K, Demircioglu MB, Duman TY, Can T, Tekin S, Azak TE, Fercan ÖZ (2018b) A probabilistic seismic hazard assessment for the Turkish territory—part I: the area source model. Bull Earthq Eng 16(8):3367–3397. https://doi.org/10.1007/s10518-016-0005-6

Specifications LBD (2012) American Association of State Highway and Transportation Officials (AASHTO). Washington, DC, USA

Tong L (2014) CPEC industrial zones and China–Pakistan capacity cooperation. Strateg Stud JSTOR 34:174–84

Treloar PJ, Potts GJ, Wheeler J, Rex DC (1991) Structural evolution and asymmetric uplift of the Nanga Parbat syntaxis, Pakistan. Himalya Geol Rundschau 80(2):411–428. https://doi.org/10.1007/BF01829374

Waseem M, Lai CG, Spacone E (2018) Seismic hazard assessment of northern Pakistan. Nat Hazards 90(2):563–600. https://doi.org/10.1007/s11069-017-3058-1

Waseem M, Khan MA, Khan S (2019) Seismic sources for southern Pakistan and seismic hazard assessment of Karachi. Nat Hazards 99(1):511–536. https://doi.org/10.1007/s11069-019-03755-5

Waseem M, Khan S, Asif Khan M (2020) Probabilistic seismic hazard assessment of pakistan territory using an areal source model. Pure Appl Geophys 177:3577–3597. https://doi.org/10.1007/s00024-020-02455-7

Waseem M, Rehman ZU, Sabetta F, Ahmad I, Ahmad M, Sabri MMS (2022) Evaluation of the predictive performance of regional and global ground motion predictive equations for shallow active regions in Pakistan. Sustainability MDPI 14(13):8152. https://doi.org/10.3390/su14138152

Wiemer SA (2001) Software package to analyze seismicity: ZMAP. Seismol Res Lett Seismol Soc Am 72(3):373–82. https://doi.org/10.1785/gssrl.72.3.373

Yeats RS, Lawrence RD (1982) Tectonics of the Himalayan thrust belt in northern Pakistan. masc

Youngs RR, Chiou SJ, Silva WJ, Humphrey JR (1997) Strong ground motion attenuation relationships for subduction zone earthquakes. Seismol Res Lett Seismol Soc Am 68(1):58–73. https://doi.org/10.1785/gssrl.68.1.58

Zaigham NA, Mallick KA (2000) Bela ophiolite zone of southern Pakistan: tectonic setting and associated mineral deposits. Geol Soc Am Bull 112(3):478–489. https://doi.org/10.1130/0016-7606(2000)112<478:BOZOSP>2.0.CO;2

Zaman S, Ornthammarath T, Warnitchai P (2012) Probabilistic seismic hazard maps for Pakistan. In: Proceedings of the 15th world conference earthquake engineering WCEE, pp 1–10

Zanchi A, Gaetani M (2011) The geology of the Karakoram range, Pakistan: the new 1: 100,000 geological map of Central-Western Karakoram. Ital J Geosci Società Geologica Italiana 130(2):161–262. https://doi.org/10.3301/IJG.2011.09

Zare M, Amini H, Yazdi P, Sesetyan K, Demircioglu MB, Kalafat D, Erdik M, Giardini D, Khan MA, Tsereteli N (2014) Recent developments of the

Rehman *et al. Progress in Earth and Planetary Science*   (2023) 10:27

Page 31 of 31

Middle East catalog. J Seismol 18(4):749–772. https://doi.org/10.1007/s10950-014-9444-1

Zhang P, Yang Z, Gupta HK, Bhatia SC, Shedlock KM (1999) Global seismic hazard assessment program (GSHAP) in continental Asia. http://hdl.handle.net/2122/1387

Zhao JX, Zhang J, Asano A, Ohno Y, Oouchi T, Takahashi T, Ogawa H, Irikura K, Thio HK, Somerville PG, Fukushima Y (2006) Attenuation relations of strong ground motion in Japan using site classification based on predominant period. Bull Seismol Soc Am Seismol Soc Am 96(3):898–913. https://doi.org/10.1785/0120050122

Publisher's Note